NASA/TM–2006–214148

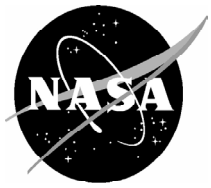

Effects of Finite Element Resolution in the Simulation of Magnetospheric Particle Motion

Rickard Hansen

December 2006

The NASA STI Program Office … in Profile

Since its founding, NASA has been dedicated to the advancement of aeronautics and space science. The NASA Scientific and Technical Information (STI) Program Office plays a key part in helping NASA maintain this important role.

The NASA STI Program Office is operated by Langley Research Center, the lead center for NASA's scientific and technical information. The NASA STI Program Office provides access to the NASA STI Database, the largest collection of aeronautical and space science STI in the world. The Program Office is also NASA's institutional mechanism for disseminating the results of its research and development activities. These results are published by NASA in the NASA STI Report Series, which includes the following report types:

- TECHNICAL PUBLICATION. Reports of completed research or a major significant phase of research that present the results of NASA programs and include extensive data or theoretical analysis. Includes compilations of significant scientific and technical data and information deemed to be of continuing reference value. NASA's counterpart of peer-reviewed formal professional papers but has less stringent limitations on manuscript length and extent of graphic presentations.
- TECHNICAL MEMORANDUM. Scientific and technical findings that are preliminary or of specialized interest, e.g., quick release reports, working papers, and bibliographies that contain minimal annotation. Does not contain extensive analysis.
- CONTRACTOR REPORT. Scientific and technical findings by NASA-sponsored contractors and grantees.
- CONFERENCE PUBLICATION. Collected papers from scientific and technical conferences, symposia, seminars, or other meetings sponsored or cosponsored by NASA.
- SPECIAL PUBLICATION. Scientific, technical, or historical information from NASA programs, projects, and mission, often concerned with subjects having substantial public interest.
- TECHNICAL TRANSLATION. English-language translations of foreign scientific and technical material pertinent to NASA's mission.

Specialized services that complement the STI Program Office's diverse offerings include creating custom thesauri, building customized databases, organizing and publishing research results . . . even providing videos.

For more information about the NASA STI Program Office, see the following:

- Access the NASA STI Program Home Page at http://www.sti.nasa.gov/STI-homepage.html
- E-mail your question via the Internet to help@sti.nasa.gov
- Fax your question to the NASA Access Help Desk at (301) 621-0134
- Telephone the NASA Access Help Desk at (301) 621-0390
- Write to:
  NASA Access Help Desk
  NASA Center for AeroSpace Information
  7115 Standard Drive
  Hanover, MD 21076–1320

NASA/TM–2006–214148

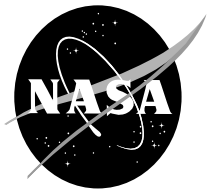

Effects of Finite Element Resolution in the Simulation of Magnetospheric Particle Motion

Rickard Hansen
NASA Goddard Space Flight Center, Greenbelt Maryland

National Aeronautics and
Space Administration

Goddard Space Flight Center
Greenbelt, Maryland 20771

December 2006

Available from:

NASA Center for AeroSpace Information
7115 Standard Drive
Hanover, MD 21076-1320
Price Code: A17

National Technical Information Service
5285 Port Royal Road
Springfield, VA 22161
Price Code: A10

Summary

This report describes the assignment posed by NASA/Goddard Space Flight Center. The assignment had three parts:

- Comparing particle trajectories computed, first in an analytically specified set of global electric and magnetic fields; and then, in the same fields as sampled onto a finite element mesh in three dimensions, with interpolation of intermediate values.
- Studying the effect of mesh spacing, resulting in an evaluation of adequate spacing resolution.
- Studying time-dependent fields in the context of substorm dipolarizations of the magnetospheric tail.

One of the aims of the assignment was to gain confidence when it comes to executing MHD-simulations, by investigating the interpolating simulations. Interpolations are much faster to do than analytical simulations. The study was designed to validate and document work that NASA has been doing to simulate test particle motions in complex three-dimensional magnetohydrodynamic (MHD) simulations of the Earth's magnetosphere.

During the whole process, the test particle code of Delcourt was used. The three-dimensional test particle trajectory code of Delcourt uses the full equation of motion, and thus, including drift velocities of second order, in order to examine in detail the motion of near-Earth (~10– 15 R_E) plasma sheet particles during substorms. The emphasis is placed on orbit features in the course of expansion phase, thus ignoring the subsequent evolution of the ion distributions produced. A total of 18 different scenarios were used during the different phases of the work. The scenarios differed in all factors, except the Tsyganenko level and the dipole tilt angle, which were kept constant except for the dynamic simulations where the Tsyganenko levels were also varied.

The results from the particle motion in an interpolated magnetic field and particle motion in interpolated magnetic and electric fields showed a very good resemblance and thus, we can be confident when it comes to executing MHD-simulations (with respect to interpolating simulations). Thus, a lot of time can be saved by using interpolation—instead of time consuming analytical simulations—in these cases. The sensitivity analysis—for the particle motion in an interpolated magnetic field and particle motions in interpolated magnetic and electric fields—in general show large improvements in accuracy between the analytical results and the precalculated results with an increased number of grid points. In some cases, more or less identical results between the analytical and the precalculated simulations were found. The decreased accuracy concerning energy could be explained by the random nature of the particle trajectories. Weighing the simulation time (the simulations take more time when increasing the number of grids) and the resulting accuracy, an optimal number of grids would probably be eight times the original number.

The few things that differed when comparing the polynomial results with the linear results—dynamic magnetic and electric fields—were generally easily corrected by increasing the time interval between the change of the Tsyganenko levels. By doing so, the time interval will make the curve much smoother and the transition less abrupt. The comparison concerning a dynamic

magnetic field showed a very good resemblance between the two cases, but when trying to add a dynamic electric field, the mathematics posed a problem. The comparison did not show enough resemblance between the two cases. The problem was finally solved, and when comparing the results of a dynamic magnetic and electric field, a very good resemblance with the analytical results was found, thus, satisfactory results were achieved.

Preface

This technical publication is based on the degree project and thesis for the MS Programme in Space Engineering, Department of Space Studies (former Kiruna Space and Environment Campus (KRM)).

The project shall demonstrate the ability to use the knowledge and skills developed by the student during the studies; characteristics such as independently analyzing and demonstrating a relatively extensive assignment in a scientifically methodical manner.

I would like to extend warm a gratitude towards everyone who has contributed to this project. The people who I would like to thank, without any order of precedence, are
–Thomas Moore, Goddard Space Flight Center / NASA, placement supervisor;
–Mei-Ching Fok, Goddard Space Flight Center / NASA;
–Manuel Buenfil, Goddard Space Flight Center / NASA; and
–Johnny Ejemalm, Department of Space Studies, academic supervisor.

Kalmar, Sweden, October, 2005

Rickard Hansen

Table of Contents

1. BACKGROUND

1.1 Assignment

The assignment was performed at NASA/Goddard Space Flight in Greenbelt, Maryland. The assignment had three parts:

- Comparing particle trajectories computed, first in an analytically specified set of global electric and magnetic fields; and then in the same fields as sampled onto a finite element mesh in three dimensions, with interpolation of intermediate values.
- Studying the effect of mesh spacing, resulting in an evaluation of adequate spacing resolution.
- Studying time-dependent fields in the context of substorm dipolarizations of the magnetospheric tail.

One of the aims of the assignment was to gain confidence when it comes to executing MHD-simulations, by investigating the interpolating simulations. Interpolations are much faster to do than analytical simulations. The study was designed to validate and document work that NASA has been doing to simulate test particle motions in complex three-dimensional magnetohydrodynamic simulations of the Earth's magnetosphere.

1.2 Theory

1.2.1 Ionosphere

The ionosphere is a neutral atmosphere that contains a source of ionization for the gases in its atmosphere. The sources of ionization include photons and energetic-particle "precipitation." The photons come primarily from the Sun as EUV/UV radiation. The process involving photons is called "photoionization" and the process involving energetic particles is called "impact ionization." Ionizing particles may come from the galaxy (cosmic rays), the Sun, the magnetosphere, or the ionosphere itself if a process for local ion or electron acceleration is operative. Precipitating energetic electrons produce additional ionizing photons within the atmosphere by a process known as Bremsstrahlung, or braking radiation. The ionization due to particles causing aurora, takes place mainly in the altitudes from 90–300 km. Cosmic rays with energies in the mega electron volt and giga electron volt intervals, cause ionization at altitudes from 90–70 km. [2]

The ionosphere consists of three major layers or regions: the D region (below 90 km), the E region (from 90–130 km), and the F region (above 130 km). The F region is usually further divided into F1 and F2 layers, because a second ledge sometimes appears in its profile below the main (F2) peak. One can think of the layers as being independently produced by the absorption of solar radiation by specific components of the neutral atmosphere, which respond differently to different parts of the incoming solar photon spectrum. The E layer is usually clearly noticeable as

a change in slope in daytime electron density profiles near 110 km. The ions in this layer are mainly O^{+2} and NO^{+}, which have been produced by UV radiation in the 100–150 nm range and solar x-rays in the 1–10 nm range. The peak density of this layer is close to the peak of the production rate for these ions. Vertical transport of ions is considered to play a minor role in the formation of this layer. The F1 layer is composed primarily of O^{+}. The maximum electron density in this layer occurs at approximately 170 km, which is close to the level of the maximum ion production by photons in the spectral range from about 17–91 nm. The F2 layer contains the main peak in the ionosphere density. This peak, due to collisions at lower altitudes, keeps the density of ionized particles down, while the density at higher altitudes is kept down by the lack of particles to be ionized. [2] This peak density is also in a region dominated by O^{+}. The lowest ionosphere, the D region, is of practical interest because of its role in commercial radio communication. The high ion-neutral collision frequencies make radio–wave absorption there important, and so the electron density is of primary concern. Only the most energetic ionization sources can penetrate to D-region altitudes. Between about 80–90 km, 0.1–1 nm x-rays from the Sun are the primary sources; the very intense Lyman-α (121.6 nm) radiation from the Sun has its peak ion production rate at about 70–80 km, and ionization of cosmic-ray particles dominates below. The predominant ions, NO^{+} and O^{+2}, can recombine with electrons, but at these low altitudes the electrons can also attach themselves to neutrals to form negative ions. In general, the variation of ionospheric density during the day depends on altitude through both the local ion composition and the source variation during the day. [1]

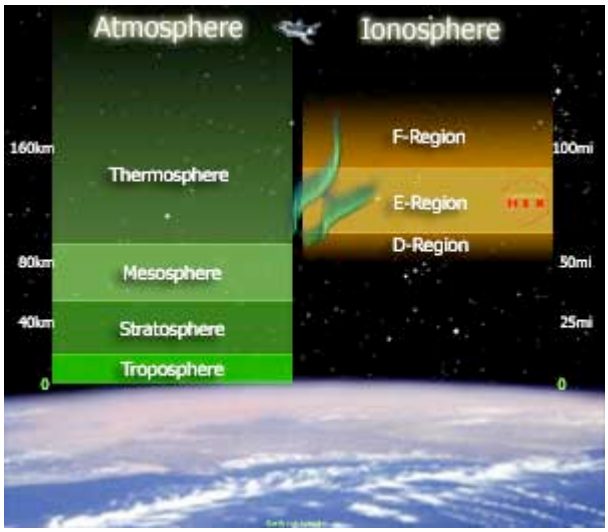

Figure 1. Ionospheric and atmospheric structure. [7]

1.2.2 Magnetosphere

The magnetosphere consists of the magnetopause, magnetosheath, and the magnetotail. The magnetopause and the magnetotail are the two regions within the Earth's magnetosphere where relatively thin sheets of electric current separate regions of different magnetic fields. The magnetopause is usually placed at a distance of 10 Earth radii on the dayside. The magnetosheath

is found within the bow shock. In the magnetosheath, the solar wind plasma flows with a subsonic speed. The magnetotail is found on the nightside. [2]

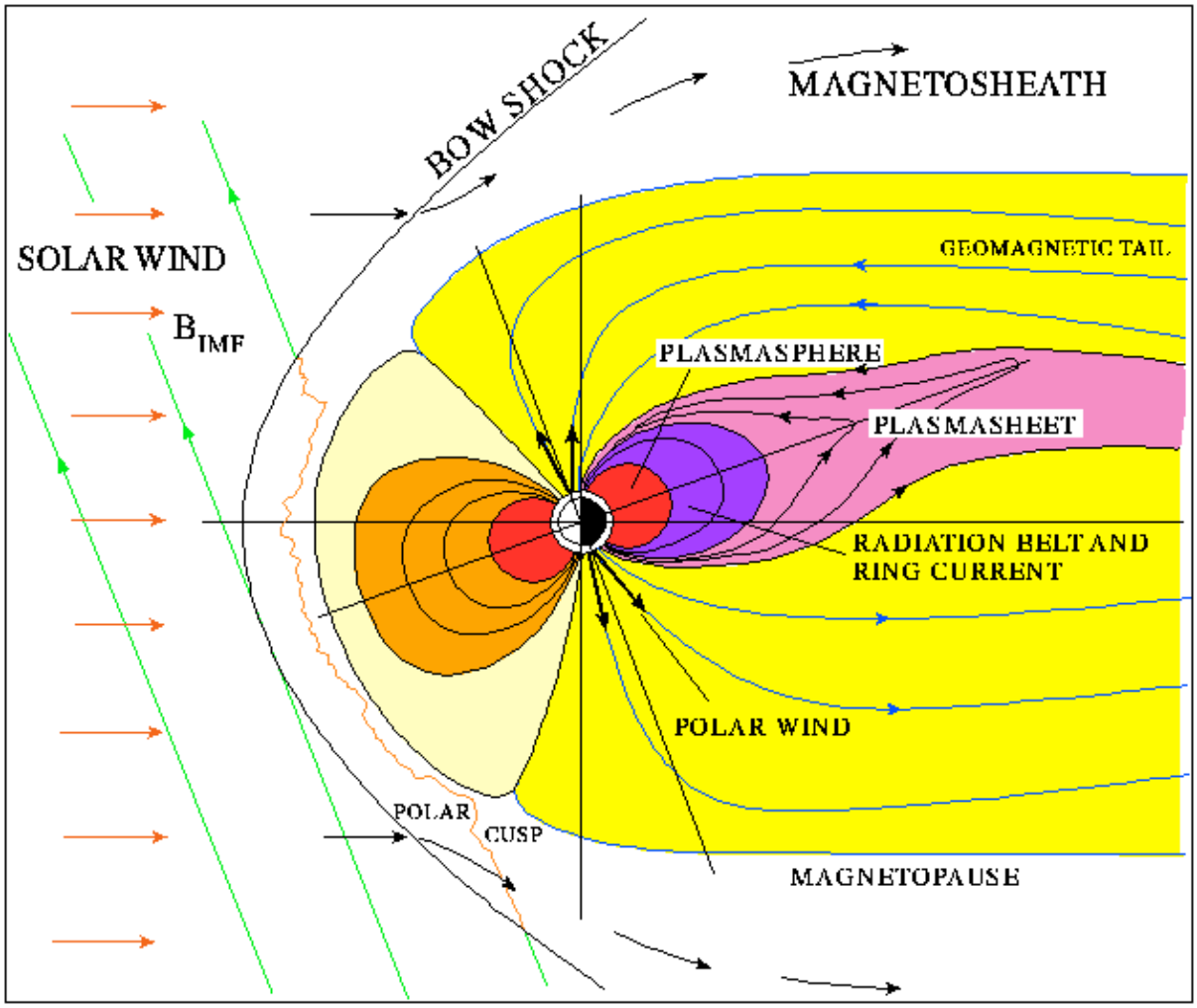

Figure 2. The Earth's magnetosphere. [7]

A current sheet can be defined as a thin surface across which the magnetic-field strength and/or direction can change substantially. Current sheets come naturally out of the frozen-in-flux concept. Collisionless plasmas do not mix easily; instead, they tend to form cells of relatively uniform plasma having a magnetic field flowing through it. These cells are separated by thin current sheets through which little or no magnetic flux crosses. The interaction between different plasma regimes occurs at these thin boundaries. Magnetic reconnection is one of these processes; see below for magnetic reconnection.

The geomagnetic tail is the region of the Earth's magnetosphere that stretches away from the Sun behind the Earth. It acts as a reservoir of plasma and energy. The energy and the plasma are released into the inner magnetosphere aperiodically during magnetospheric substorms. A current sheet is situated in the center of the tail, embedded within a region of hot plasma—the plasma

sheet—which separates two regions called the tail lobes. The two tail lobes connect magnetically to the two polar regions of the Earth and are identified as the north and south lobes.

The highly stretched magnetic-field geometry of the Earth's magnetotail implies a westward tail current across the center of the tail, near the equatorial plane. The inner magnetosphere contains a ring current, which flows westward in approximate circles centered on the Earth. Additional partial-ring currents also flow partway around the Earth in the middle magnetosphere. Birkeland currents connect the ends of the partial rings to the ionosphere, where conduction currents can complete the circuit. Additional Birkeland currents connect to the tail and magnetopause boundary layer. [1]

The magnetopause is the upper boundary of the magnetosphere. It separates the geomagnetic field and plasma of primarily terrestrial origin from solar-wind plasma. In the simplest approximation, the magnetopause can be considered as a boundary separating a vacuum magnetic field from plasma. Three distinct types of magnetopause boundary layers are recognized:

- **The Low-Latitude Boundary Layer** (LLBL), a region that contains a mix of magnetosheath and magnetosphere plasma, and within which plasma flows can be found in almost any direction, but are generally intermediate between the magnetosheath flow and magnetospheric flows. The entry layer is found in the region where the magnetic null or cusp occurs in a closed magnetopause model and extends about 3h either side of noon. The plasma is characteristic of the magnetosheath, but the flows are low-speed and disordered.
- **The High-Latitude Boundary Layer** (HLBL), or plasma mantle, is found at higher latitudes tailward of the cusp and entry layer. Within HLBL flows are always tailward, but flow speed, density, and temperature all decrease away from the magnetopause. In general, the HLBL is spatially uniform, with a gradual transition from magnetosheath to lobe properties. It often has no distinct inner edge, in sharp contrast to the LLBL, which usually has a very distinct inner edge. The entry layer and plasma mantle are generally agreed to be on open magnetic-field lines. They are populated by a mixture of magnetosheath plasma, that entered the magnetosphere along open field lines in the cusp and ionospheric plasma, which flowed up from the cusp and polar cap in an upward flow known as the "polar wind." Reconnection is assumed to occur at the nose of the magnetopause. Magnetosheath particles flow along the newly opened field lines. The particles mirror as they encounter the stronger magnetic field nearer the Earth. After mirroring, they move back up the field line, joined by lower-energy ionospheric particles. The field line has meanwhile convected tailward to become a lobe field line, still near the magnetopause, or a mantle field line. Lower-energy particles move slower and thus, take longer to reach a given distance downtail. In this longer time, the field line will have convected farther from the magnetopause.
- **The Plasma-Sheet Boundary Layer** (PSBL) forms the boundaries between the plasma sheet and the two tail lobes. Within this boundary layer, plasma-number density and temperature are intermediate between lobe and central plasma sheet values, but its most characteristic feature is sustained field-aligned ion and electron flows, directed both Earthward and tailward. The PSBL is formed of plasma that has just been accelerated in a reconnection region.

The most important currents that give rise to the magnetospheric magnetic field are those that flow inside the Earth. The Earth's field is effectively a perfect dipole at distances more than about two Earth radii from the center of the Earth. Plasma flows over the polar–regions from noon toward midnight and then back toward the dayside at somewhat lower latitudes, corresponding roughly to the auroral zone, on both the dawn and dusk sides (="convection").

1.2.3 Magnetic Reconnection

Magnetic reconnection is a process that can take place only if the magnetic-field lines being convected with the fluid breaks down. Magnetic-field lines enter the diffusion region from the top and bottom, and instead of being annihilated, they leave from both sides. In the process, they are cut and reconnected to different partners. Plasma that was originally on different flux tubes, coming from different regions, now finds itself on a single flux tube in total violation of the frozen-in-flux theorem. Previously, the current sheet separated two magnetic-field regions; now magnetic flux crosses the current sheet. In other words, we now have an open boundary with a finite normal magnetic-field component, as opposed to the previous closed boundary. Plasma can cross the boundary by following flux tubes.

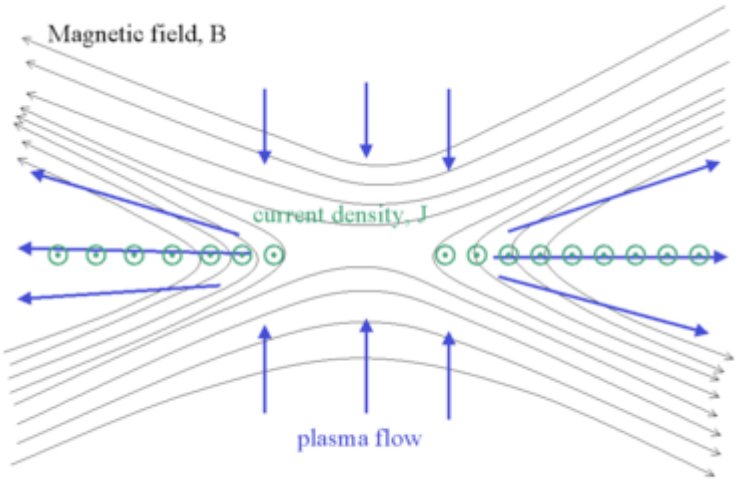

Figure 3. Magnetic reconnection at the diffusion region. [8]

1.2.4 Ionosphere–Magnetosphere Coupling

The role of the ionosphere as a plasma source for the magnetosphere has been increasingly considered since the discovery of energetic O^+ in the auroral zone. Observations throughout the magnetosphere have revealed the presence of ionospheric ions in all regions: auroral zone, plasmasphere, plasma sheet and lobe, magnetosheath, and boundary layers. [6] The key electrodynamic element in the physical coupling between the ionosphere and the magnetosphere is the current that flows along field lines between the two regions.

For typical steady conditions, the inner edge of the plasma sheet can effectively shield the inner magnetosphere, and the low-latitude and mid-latitude ionosphere to which it is connected, from the convection electric field. Shielding by the inner edge of the plasma sheet is frequently ineffective. Time variations in the applied convection potential or other magnetospheric parameters can cause temporary penetration of the shielding. It is also possible that the plasma

sheet is sometimes incapable of effective shielding for longer periods. Furthermore, neutral winds generated by magnetospheric activity can cause significant electric fields at low and middle latitudes in the ionosphere. Significant potential drops are observed to occur along auroral-zone magnetic-field lines. These potential drops usually occur in regions of strong upward field-aligned current.

Two major processes cause magnetospheric particles to be lost in the Earth's atmosphere, namely, pitch-angle, scattering, and charge exchange. A particle that conserves its first adiabatic invariant is likely to be lost to the atmosphere if its mirror magnetic field exceeds the magnetic field at a few hundred kilometers altitude. Auroral-particle precipitation proceeds primarily because plasma waves change particle pitch angles in violation of the first adiabatic invariant. Pitch-angle scattering occurs much more slowly in the radiation belts than in the plasma sheet, and radiation-belt particles can orbit the Earth for days, weeks, or months, depending on their species, energy, and location. [1]

Cold plasmas from the ionosphere contribute to the hot plasmas of the magnetosphere. On openly convecting field lines, polar wind occurs continuously as convection opens the field lines and empties their accumulations into the polar lobes and downstream solar wind, so that they never reach equilibrium pressures and are therefore called "refilling flows." The outer plasmasphere has been shown to flow Sunward during magnetospheric disturbances and these cold plasmas have been discovered to be present in the subsolar low-latitude magnetopause region under a wide variety of conditions. When strong convection drains away part of the plasmasphere, the supply of plasma is enhanced in a transient way by the rapid release of accumulated plasma. Under steady conditions, however, the plasmasphere remains trapped and the magnetosphere is supplied only from the higher-latitude polar wind regions. The contribution of ionospheric light ions to magnetospheric hot plasmas is not as well established and is complicated by the difficulty of discriminating protons of solar or geogenic origin.

The light ion auroral outflows have fluxes similar to polar wind, while the heavy ion outflows have fluxes that range from much less than, to much greater than, polar wind outflows depending on the free energy available. [3] Heavy ions are important during magnetospheric storms, when the dissipation of energy in the ionosphere proper is substantial. Part of this energy goes into energization of heavy ions sufficient to overcome their gravitational binding to the Earth. Other research has shown that the supply of ionospheric plasma to the plasma sheet, especially heavy O^+ plasma, is not only important, but is strongly modulated by convection as driven by the Interplanetary Magnetic Field. [3]

1.2.5 Adiabatic Invariants

If the changes in the magnetic field encountered by a particle within a single gyration orbit, will be small compared with the initial field, then the particle's magnetic moment, μ, is given by

$$\mu = \frac{m v_{\perp}^2}{2 \cdot B}, \qquad (1)$$

where m is the mass of the particle, $v_\perp$ is the velocity perpendicular to the magnetic field, and the quantity B is the magnetic field. The magnetic moment will remain constant, and the quantity μ is also called the first adiabatic invariant. Adiabatic in this case refers to the requirement that μ may not remain invariant or unchanged unless the parameters of the system—such as its field strength and direction—change slowly. The second adiabatic invariant is also called the bounce invariant, which is given by

$$J = \oint p_{\|} dl = 2 \int_{m_2}^{m_1} m v_{\|} dl \,, \tag{2}$$

where $p_{\|}$ is the component of the momentum along the magnetic field, $v_{\|}$ is the component of the velocity along the magnetic field, l is the distance along the field line, and m_1 and m_2 are the locations of the particle's mirror points.

What this means is that a particle trapped on magnetic field lines and conserving its adiabatic invariants will be confined to a surface specified by the distance l to the equatorial crossing of the field line over half a bounce from mirror point m_1 to m_2.

As a particle bounces and drifts in a magnetic field that varies slowly along its orbit, it traces out a so-called "drift shell." The flux that is enclosed by this shell is the same for any surface that intersects along a closed curve. If the field changes slowly (on time scales long compared with the time required for the particle to drift fully around the field), the flux enclosed by the drift shell will remain unchanged. The third adiabatic invariant is defined as the magnetic flux enclosed by the drift shell of a particle. [1]

1.2.6 Magnetohydrodynamics (MHD) Theory

The relevant fluid equations for plasmas are the equations of hydrodynamics, but because electric and magnetic fields and currents are always important in plasmas, one must include their effects as well. This means that the equations of magnetohydrodynamics (MHD) must be introduced. The equations incorporate familiar mechanical laws and also account for electromagnetic properties.

The continuity equation, which states what happens to the number density of the fluid as it moves from one place to another, says that the number of particles can change only if there are particle sources (S_s) or losses (L_s) which are given by

$$\frac{\partial n_s}{\partial t} + \nabla \cdot n_s \mathbf{u}_s = S_s - L_s \,, \tag{3}$$

where n_s is the number density, t is the time, $\boldsymbol{u}_s$ is the flow velocity, S_s is the particle sources, and L_s is the particle losses.

The momentum equation is given by

$$(\frac{\partial(\rho_s \mathbf{u}_s)}{\partial t} + \nabla \cdot (\rho_s \mathbf{u}_s \mathbf{u}_s)) = -\nabla p_s + \rho_{qs}\mathbf{E} + \mathbf{j}_s \times \mathbf{B} + \rho_s \mathbf{F}_g / m_s, \quad (4)$$

where ρ_{qs} is the charge density, $\mathbf{j}_s$ is the current density, ρ_s is the mass density, p_s is the pressure force, $\mathbf{E}$ is the electric field, $\mathbf{B}$ is the magnetical field, $\mathbf{F}_g$ is the non- electromagnetical forces (such as gravitational forces), and m_s is the particle mass.

In order to consider the equations that describe how current and charge density affect the magnetic and electric fields, Maxwell equations are used. Included in the Maxwell equations is Poisson's equation—which deals with the electric field—which is given by

$$\nabla \cdot \mathbf{E} = \rho_q / \varepsilon_0, \quad (5)$$

where ρ_q is the net charge density and ε_0 is the permittivity of free space.

Faraday's law—which deals with the electric field—is given by

$$\frac{\partial \mathbf{B}}{\partial t} = -\nabla \times \mathbf{E}. \quad (6)$$

Ampère's law—which relates the magnetic field to the net current—is given by

$$\nabla \times \mathbf{B} = \mu_0(\mathbf{j} + \varepsilon_0 \frac{\partial \mathbf{E}}{\partial t}), \quad (7)$$

where μ_0 is the permeability of free space and $\mathbf{j}$ is the net current.

The requirement that $\mathbf{B}$ is divergenceless, given by

$$\nabla \cdot \mathbf{B} = 0. \quad (8)$$

Lorentz-force law is given by

$$\mathbf{F} = q(\mathbf{E} + \mathbf{u} \times \mathbf{B}). \quad (9)$$

When $\mathbf{E} + \mathbf{u} \times \mathbf{B} = 0$ is valid, one can demonstrate that in MHD fluid flow, the magnetic flux can be frozen into the fluid. The frozen-in-flux conditions tells us that if we follow the fluid initially on a certain surface as it moves through the system, the flux through the surface will remain constant even as the surface changes its location and its shape. [1]

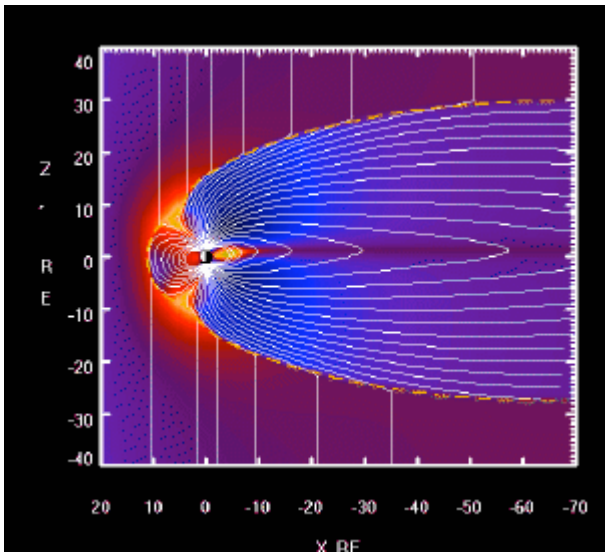

Figure 4. MHD simulation of Earth's magnetosphere. [9]

2. Method and Results

2.1 Computer Tools and Codes Used

During the work, the LINUX operating system was used. The simulations and calculations were done using FORTRAN-codes. The graphical presentations were made by using Interactive Data Languages (IDL) code, which is generally used by NASA.

2.1.1 FORTRAN

The name FORTRAN is derived from FORmula TRANSlation, indicating that the language was intended from the start for translating scientific equations into computer code. The first version of the FORTRAN language was developed during the years 1954–1957 by IBM. When FORTRAN was introduced, it was a success from the start as it made programming so much easier than machine language. FORTRAN has gone through changes throughout the years, being updated in 1962, 1977, 1990, 1996, and at present (FORTRAN 2000). [4] FORTRAN is still indeed a living language and still very much in use in the scientific world. One of the reasons why FORTRAN is still in use is that so much scientific material is written in FORTRAN and to translate this into another language would simply cost too much.

2.1.2 IDL

IDL stands for Interactive Data Language, which is an array-oriented data analysis and visualization environment. The first version of IDL was released in 1981. Since then, IDL has emerged from its roots in the astronomical and space sciences to become a widely used tool in research, educational, and commercial settings in areas as diverse as the Earth sciences, medicine, physics, and engineering tests and analysis. IDL is used, for example, when analyzing and visualizing images from the Hubble Space Telescope. One of the strengths of IDL is its support for a variety of hardware and operating systems combinations. [5]

2.1.3 Test Particle Code of Delcourt

During the entire process, the test particle code of Delcourt was used. The three-dimensional test particle trajectory code of Delcourt uses the full equation of motion and thus it includes drift velocities of the second order, in order to examine in detail the motion of near-Earth (~10–15 R_E) plasma sheet particles during substorms. The emphasis is placed on orbit features in the course of the expansion phase.

In the test particle code of Delcourt, the magnetic field model of Tsyganenko 89 was used. The magnetic field **B** was therefore considered to be the sum of the Earth dipole, $\mathbf{B}^{dip}$, and an external contribution, $\mathbf{B}^{ext}$. In order to include the electric field induced by the time-varying magnetic

field, a vector potential **A** associated with the perturbation $\mathbf{B}^{\text{ext}}$ was calculated. The instant magnetic field and induced electric field in a position **r** are given by

$$\mathbf{B}(\mathbf{r},t) = \mathbf{B}^{dip}(\mathbf{r}) + curl\left[\mathbf{A}(\mathbf{r},t)\right] \tag{10}$$

and

$$\mathbf{E}^{ind}(\mathbf{r},t) = -\partial\mathbf{A}(\mathbf{r},t)/\partial t\ . \tag{11}$$

The full equation of motion was used in order to track all ion drift paths and was given by

$$\mathbf{r}^{"} = (q/m)\left[\mathbf{E} + \mathbf{r}^{'} \times \mathbf{B}\right] + \mathbf{g}\ , \tag{12}$$

where **r** is the instant position of the particle, q is the charge of the particle, m is the mass of the particle, **g** is the gravitation, and **E** is the combined induced and polarization electric fields.

Equation (12) was integrated using the Runge-Kutta technique of the fourth order. The above described set of equations, was solved in the FORTRAN-code used during all simulations (with conditional conditions being fulfilled).

During the expansion phase of a substorm, single-particle trajectory simulations demonstrate increased Earthward convection of low-latitude plasma in the midtail region (~10 R_E). They indicate possible dramatic ion accelerations, mainly in the perpendicular direction. They underline the determining role of the particle drifts, which have usually been considered negligible and show clearly the following two effects:

1. A possible creation of new high-altitude mirror points results from large centrifugal accelerations across the magnetospheric field lines and is controlled by particle parallel velocity.
2. A possible breaking of the first adiabatic invariant relates to intense polarization drifts and depends on particle mass and/or charge state via gyroperiod.

Systematic orbit calculations show that the low-latitude populations are most affected by the convection of the geomagnetic tail and reveal possible dramatic accelerations of the particles. These trajectory results are of relevance to explain various storm time signatures at geosynchronous altitudes and provide a populating mechanism for the ring current region. [11]

2.2 Particle Motions in Interpolated Magnetic Field

The first simulations were aimed at getting the results of the analytical cases to fit the results of the precalculated cases, with only a magnetic-field added (only co-rotation electric field was included) and with no variations in time. Tsyganenko level 2 in the Tsyganenko 89 model (describing geomagnetic conditions) was used. Tsyganenko's magnetospheric magnetic field model of 1989, takes into account the effect of warping the tail current sheet in two dimensions due to the geodipole tilt, as well as spatial variations of the current sheet thickness along the Sun–

Earth and dawn–dusk directions. The corresponding analytic forms for the magnetic field components are obtained using an indirect approach in a two-stage procedure. [12] The tilt angle of the dipole was set to 0°, the simulated particle was a proton, the initial particle energy was set to 1000 eV, and the initial Magnetic Local Time (MLT) was on the nightside during all simulations. MLT at a given location is determined by the angle subtended at the geomagnetic axis between the geomagnetic midnight meridian and the meridian that passes through the location. The following factors were varied: initial distance to Earth, initial magnetic latitude, initial pitch angle, and initial gyrophase. See Tables 1 and 2, for a full description of the simulated scenarios that were used throughout the report.

In order to get the results of the analytical cases to fit the results of the precalculated cases, the following measures were taken:

1. Only the co-rotational part of the electric field was kept, the convectional part was set to zero.
2. Only the external field was interpolated, the dipole field was then added on.
3. A spherical grid-system was used.

A total of 18 different scenarios were used during the different phases of the work. The scenarios differed in all included factors except the Tsyganenko level and the dipole tilt angle, which were kept constant except for the dynamic simulations where the Tsyganenko level was also varied. The Tsyganenko level describes the geomagnetic conditions using a scale from 1 to 6, where 1 equals quiet geomagnetic conditions and 6 equals the most disturbed geomagnetic conditions.

a. The dipole tilt angle is the angle between the geomagnetic dipole and the plane orthogonal to the Earth–Sun line (varies within a range from -35° to +35°).
b. The magnetic local time will vary between 00 hours to 24 hours.
c. The magnetic latitude will vary between -90° to +90°.
d. The pitch angle is the angle between **v** and **B**.
e. The pitch angle will vary between 0° and 180°.
f. The gyrophase will vary between 0° and 360°.

Table 1. Scenario 1 through 9

Scenario	1	2	3	4	5	6	7	8	9
Tsyganenko level	2	2	2	2	2	2	2	2	2
Dipole tilt angle (°)	0	0	0	0	0	0	0	0	0
Initial geodistance (RE)	2	4	6	8	10	12	14	6	2
Initial magnetic local time (h)	20	20	23	23	23	23	23	23	23
Initial magnetic latitude (°)	45	45	45	45	45	45	45	10	10
Initial energy (eV)	1000	1000	1000	1000	1000	1000	1000	1000	1000
Initial pitch angle (°)	45	45	45	45	45	45	45	45	45
Initial gyrophase (°)	45	45	45	45	45	45	45	45	45

Table 2. Scenario 10 through 18.

Scenario	10	11	12	13	14	15	16	17	18
Tsyganenko level	2	2	2	2	2	2	2	2	2
Dipole tilt angle (°)	0	0	0	0	0	0	0	0	0
Initial geodistance (RE)	12	2	6	12	2	6	12	6	12
Initial magnetic local time (h)	23	23	23	23	23	23	23	23	23
Initial magnetic latitude (°)	80	45	45	45	45	45	45	10	10
Initial energy (eV)	1000	1000	1000	1000	1000	1000	1000	2000	3000
Initial pitch angle (°)	45	10	20	80	45	45	45	45	45
Initial gyrophase (°)	45	45	45	45	10	20	80	45	45

Very good results were achieved for the simulated scenarios, where the energy in both the analytical and the precalculated cases were kept relatively constant and the particle trajectories showed very similar results, which was desirable. See Figures 5 and 6 for an example (Scenario 4). As seen from Figures 5 and 6, the energy is kept fairly constant in both cases. The pitch angle, magnetic moment, and to a lesser degree, the kappa-value are very similar in both cases. The kappa-value is the square root of the magnetic field curvature radius to the particle gyroradius. [13] The appearance of the trajectories has similarities.

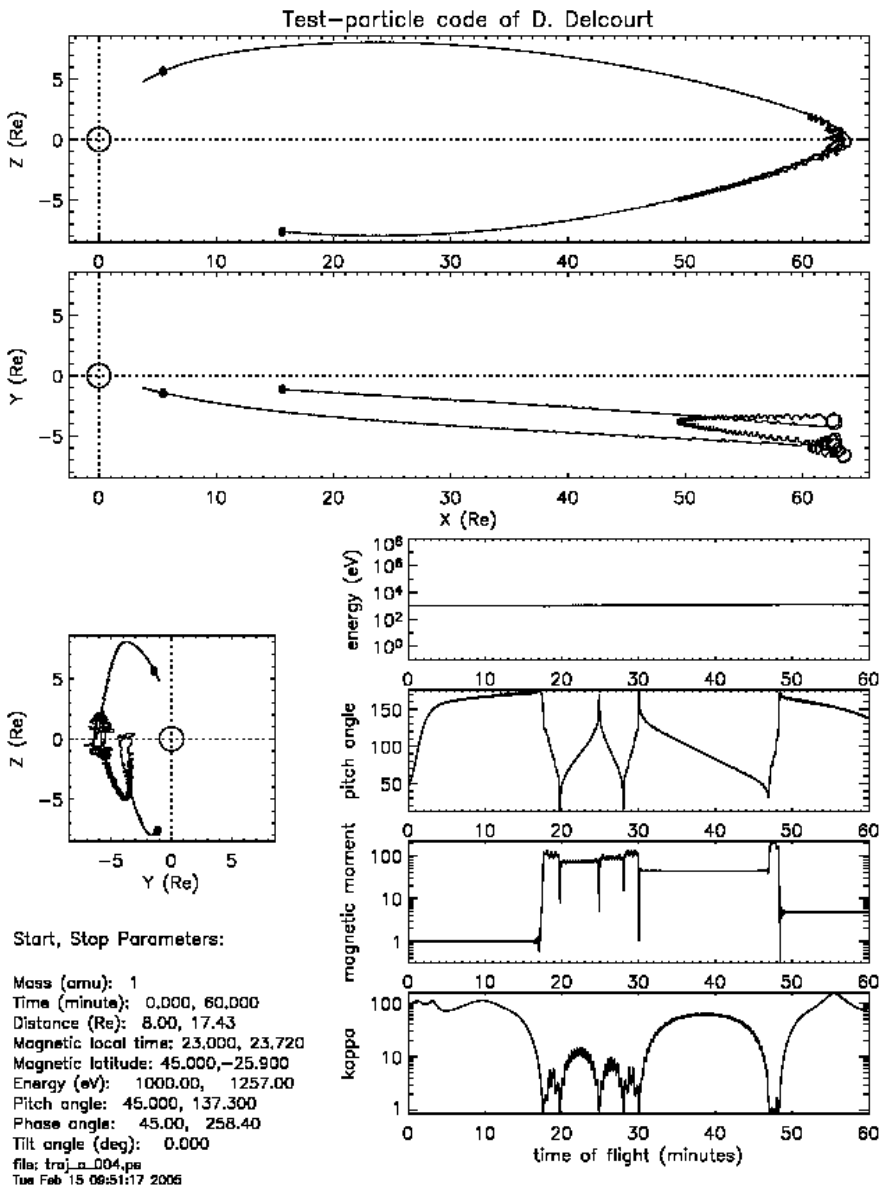

Figure 5. Results from the analytical case, interpolated magnetic field (Scenario 4).

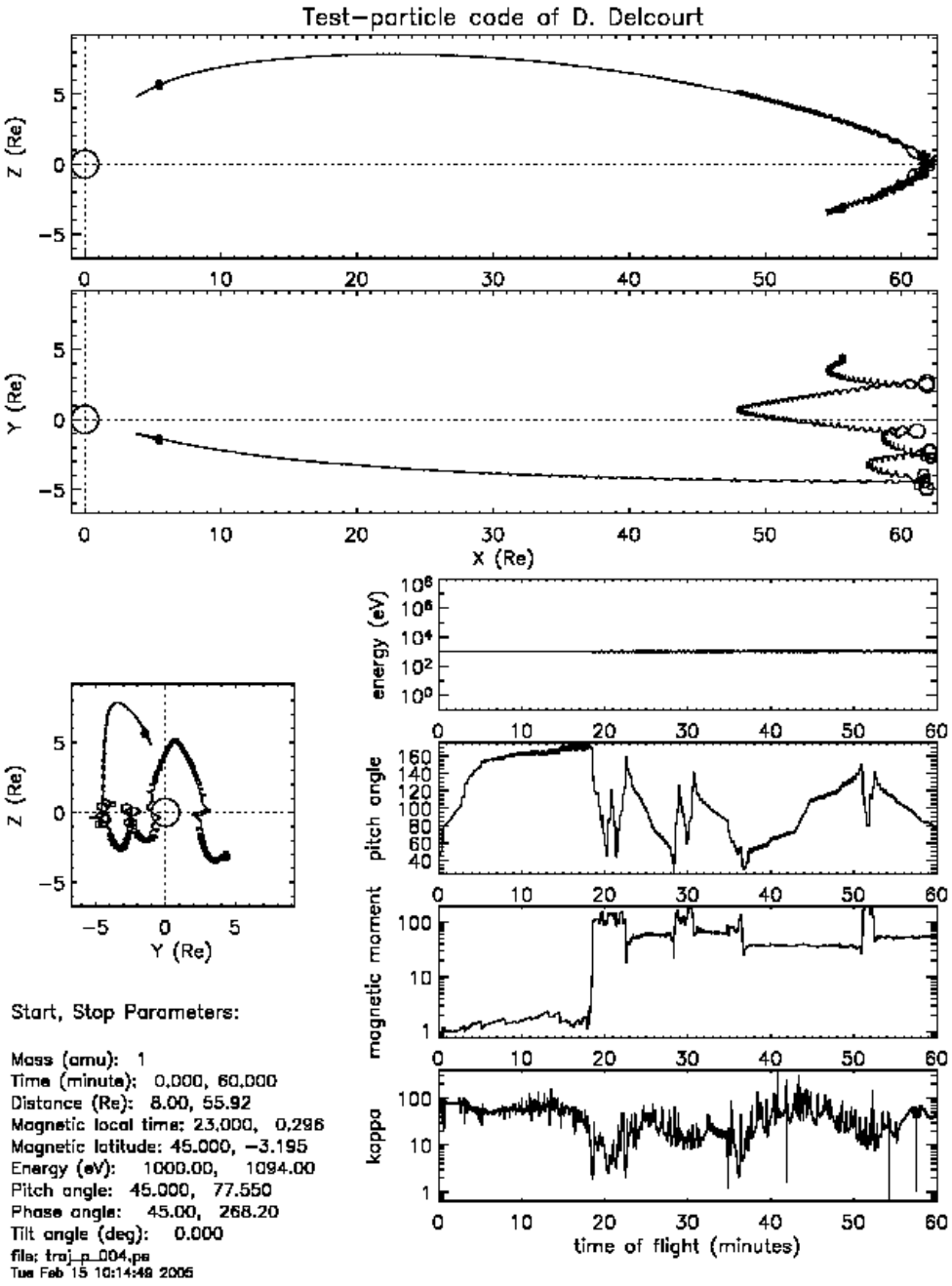

Figure 6. Results from the precalculated case, interpolated magnetic field (Scenario 4).

2.3 Particle Motions in Interpolated Magnetic and Electric Fields

The work now continued with adding an electric field. A FORTRAN-code was developed, which generates an electric field in accordance to Stern–Volland. The Stern–Volland electric field model is K_p-dependent. Later models are also time-varying with respect to the convection electric field. [10] During the development of the code, the region below the ionosphere was assumed to

be a dipole. The generated electric field was used in the simulation code, where the co-rotational part was also activated. Particle trajectories with initial conditions listed in Tables 1 and 2 are calculated in the precalculated magnetic and electric fields. The trajectories are compared with those with the same initial conditions, but are calculated in analytical fields.

In order to get an idea of the procedure of the simulations, Figure 7 will give an idea of how the different codes were used during the simulations.

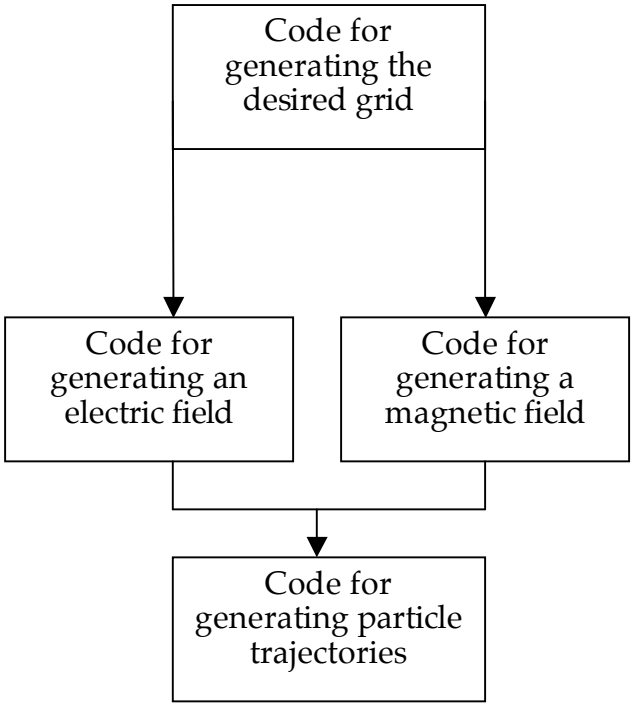

Figure 7. The scheme of the different codes involved.

The results of the analytical and the precalculated cases were compared. Minor adjustments concerning the sampling interval of the electric field were made in order to improve the resemblance between the cases. The results showed a very good resemblance, concerning energy, pitch angle, magnetic moment, kappa-value, and the appearance of the trajectory. See Figure 8 for an example (Scenario 3).

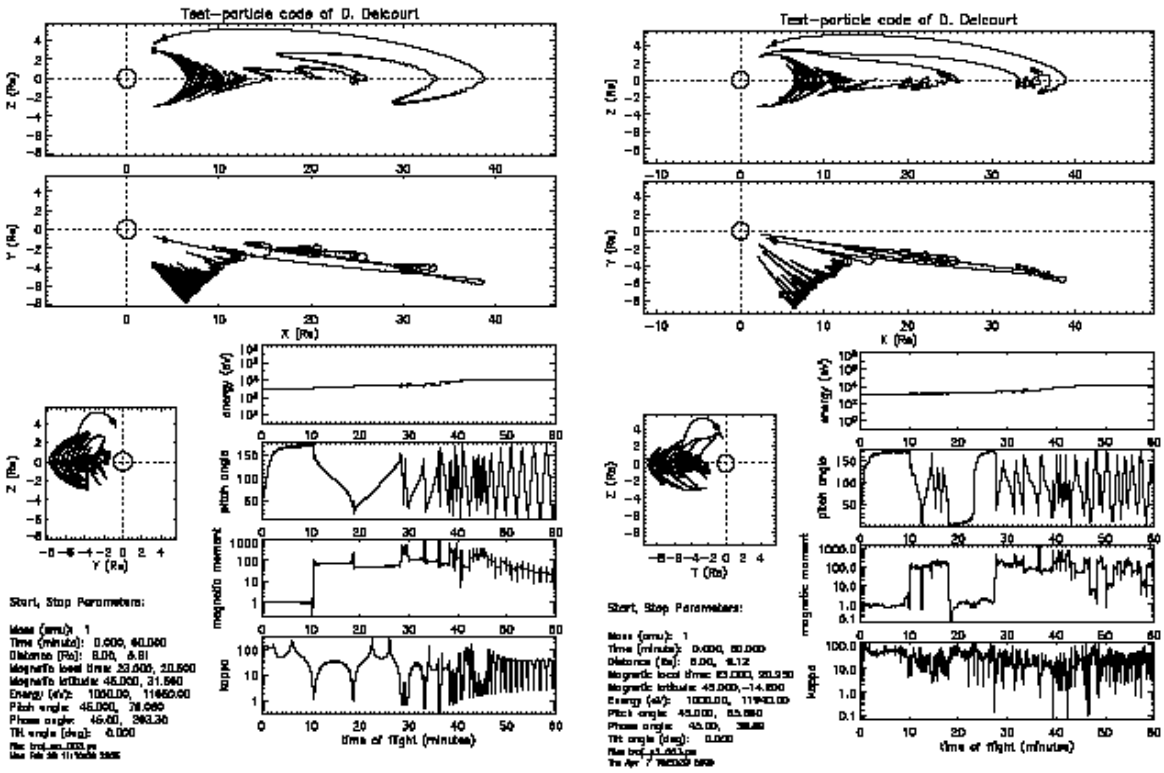

Figure 8. Analytical case to the left and the precalculated case to the right (Scenario 3).

2.4 Dynamic Magnetic and Electric Fields

During the simulations, while varying the magnetic and electric field, a linear and a polynomial transition between Tsyganenko level 5 to level 2 was used. The results of the two different transitions were then examined in order to look for differences in the resulting parameters. As for the linear and polynomial transition, we use the function *B(t)* given by

$$B(t) = B(t_0) + F(t)(B(t_f) - B(t_0)), \tag{13}$$

where the linear transition uses:

$$F(t) = \frac{t - t_0}{t_f - t_0}, \tag{14}$$

while the polynomial transition—in this case—uses:

$$F(t) = 10 \cdot (\frac{t - t_0}{t_f - t_0})^3 - 15 \cdot (\frac{t - t_0}{t_f - t_0})^4 + 6 \cdot (\frac{t - t_0}{t_f - t_0})^5. \tag{15}$$

After comparing the simulations with the two different transitions, the work started on developing a trajectory code where a dynamic magnetic field (level 5 to level 2) and interpolation (precalculated) was used. When the results were found to be good enough, the electric field was to be added on.

When comparing the results of the linear transition and the polynomial transition, a very good resemblance was found (nearly identical resemblance), concerning pitch angle, kappa-value, and the appearance of the trajectory. The only things that differed were the magnetic moment—where the linear transition results in a sudden and powerful change of the magnetic moment, which depends on the sudden change in the electric field—and the energy to a certain amount. In one case (Scenario 8), the polynomial transition showed a sudden and powerful change in the kappa-value, which the corresponding linear transition did not show. The time interval of the transition was increased in this case from 60 to 600, which resulted in the powerful change of the kappa-value disappearing. Increasing the time interval means that the transition is being made more smoothly. See Appendix 1 for the linear and the polynomial transition for Scenario 8. See Appendix 2 for the linear and the polynomial transition for Scenario 8, when increasing the time interval to 600.

When comparing the results of a dynamic magnetic field, a very good resemblance with the analytical results was found, except for one scenario (Scenario 10). In this scenario, the particle was found in the polar cusp and this is where the magnetic field has discontinuities, which will make interpolation hard to achieve. See Appendix 3 for graphs of Scenario 10.

When the electric field was added, the newly generated electric field was checked against the earlier electric field by checking the potential in a certain point. The values of the potential in a point were found to be the same for both fields. See Figure 9, for a view of the electric fields in X-Z-plane, e_x-direction.

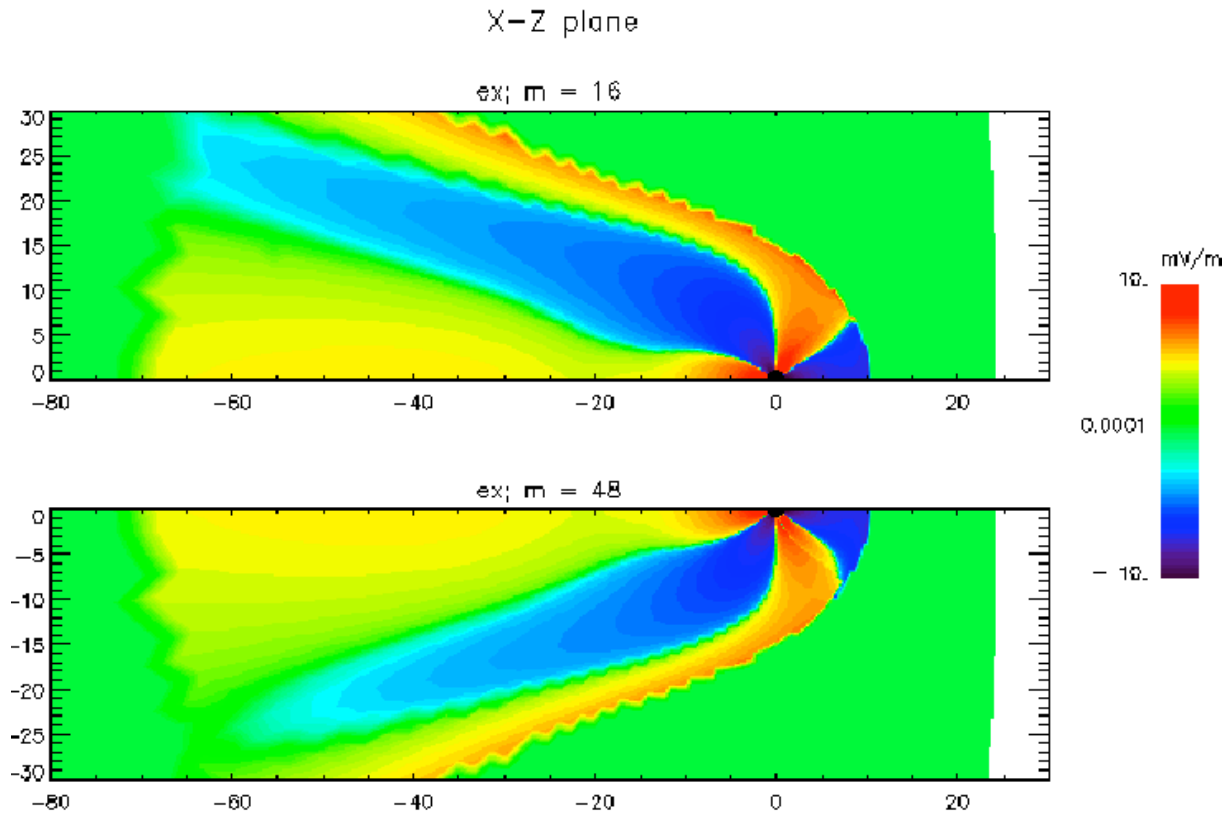

Figure 9. The electric fields in X-Z-plane and e_x-direction.

Simulations were now conducted with a dynamic magnetic and electric field added on. The results between the analytical and the interpolated (precalculated) simulations were found to have good resemblances. The resemblances concerning the electric field, however, were not found to be adequate, thus the work continued with the electric field. The problem was how to calculate the expression given by

$$\int (E_i \bullet B) ds \,, \tag{16}$$

without field line tracing. Equation (16) is found in the expression for the total E-field, given by

$$E = -\nabla (P + \int (E_i \bullet B) ds) + E_{i\perp} \,, \tag{17}$$

where P is the electrostatic potential (obtained from mapping to the ionosphere), E_i is the inductive electric field, and B is the magnetic field. The problem was solved in the following way: the total E-field was precalculated during the transition between the two levels, calculating the E-field at a 3 second interval. The particle trajectory was calculated by doing temporal and spatial interpolation to find the E-field at a particular time and location along the trajectory. When comparing the results of a dynamic magnetic and electric field, a very good resemblance with the analytical results was found. See Figures 10 and 11 for an example (Scenario 1).

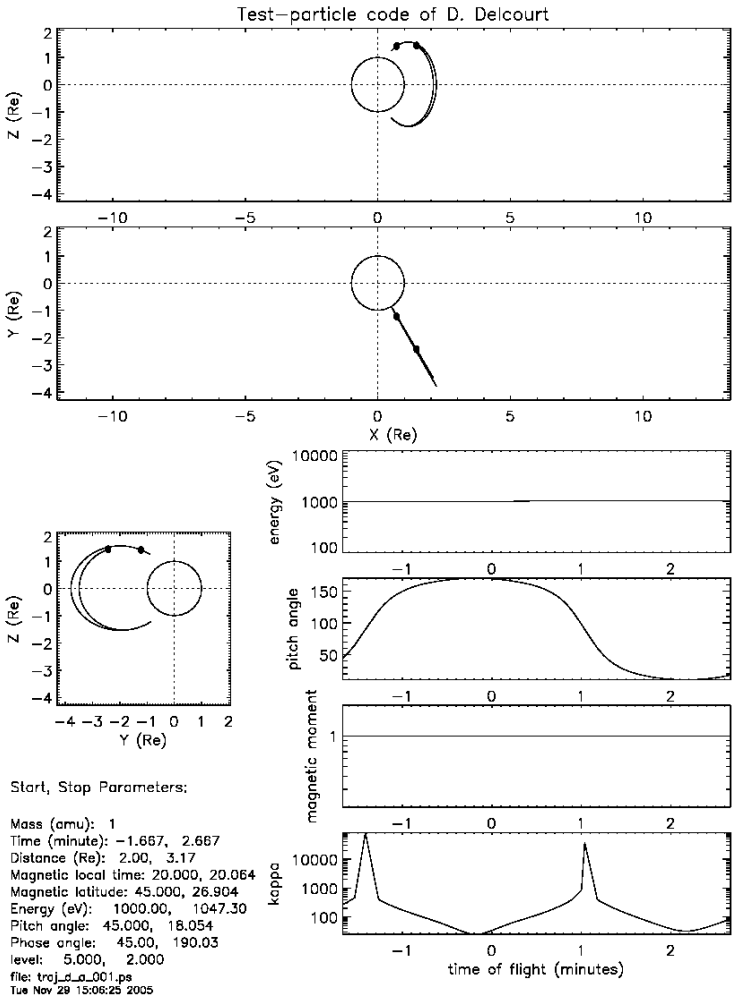

Figure 10. Analytical case (Scenario 1).

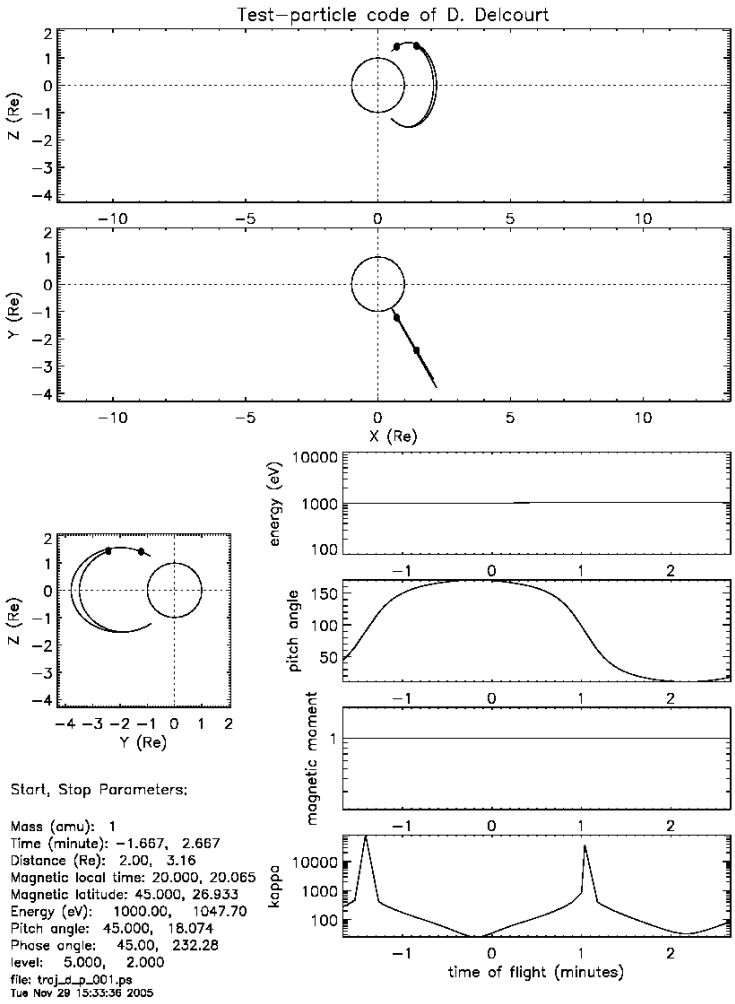

Figure 11. Precalculated case (Scenario 1).

3. Analysis and Discussion

3.1 Particle Motions in Interpolated Magnetic Field

The measures taken were found to be adequate to get the analytical cases to fit the results of the precalculated cases. The results compared were the trajectories, energy, pitch angle, magnetic moment, and the kappa-value. The most interesting input values were varied in the different scenarios. They were varied within a quite diverse range of numbers (see Tables 1 and 2). Still, the results showed very good resemblance between the analytical cases and the precalculated cases.

3.2 Particle Motions in Interpolated Magnetic and Electric Fields

The measures taken were found to be adequate to get the analytical cases to fit the results of the precalculated cases. The results compared were the trajectories, energy, pitch angle, magnetic moment, and the kappa-value. The same accuracy in resemblance was received as for the case with the interpolated magnetic field.

3.3 Sensitivity analysis

Simulations were carried out for all scenarios—with particle motions in interpolated magnetic and electric fields—using grid systems, 8 times the original number of grids, 27 times, and finally half the number of grids. A simulation using 64 times the original number of grids was stopped as the computer crashed. When developing the grid systems, the given grid points from the original grid system were used. We obtained the new grid points using linear interpolation. See Figures 12 and 13 for the original grid system and the grid system with 8 times the original number of grids.

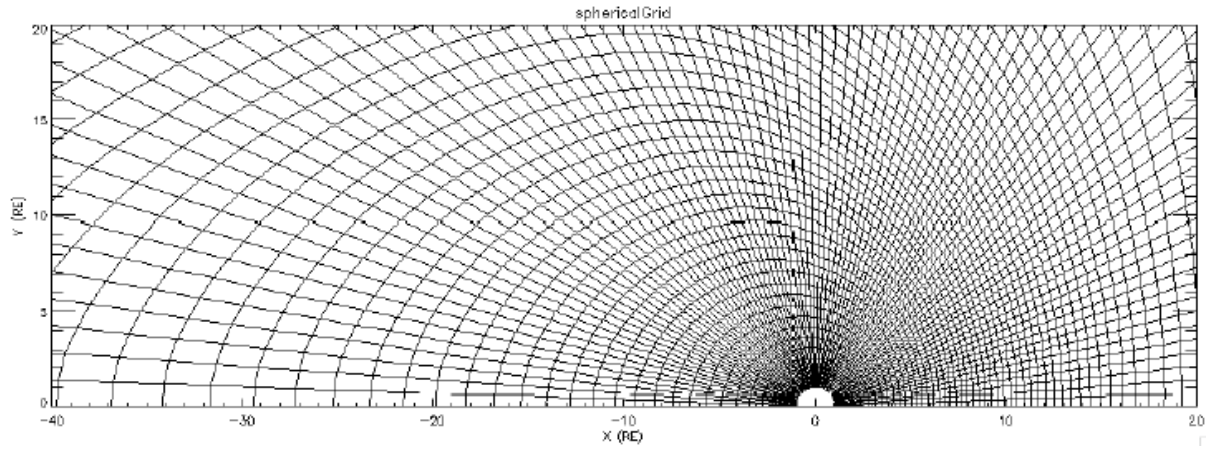

Figure 12. The original grid system.

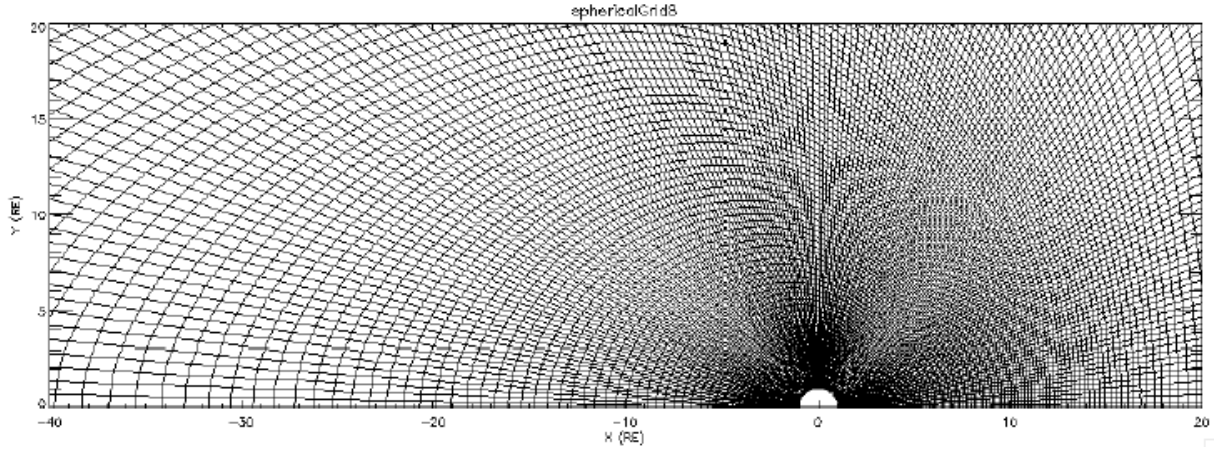

Figure 13. The grid system 8 times the original number of grids.

The following results were received for the different scenarios:

Scenario 1: The resemblance to the analytical case gets better when it comes to pitch angle, magnetic moment, and the appearance of the trajectory, but unfortunately, in the case of a grid 27 times the original amount, the particle precipitated shortly after release and no conclusions can be made.

Scenario 2: The resemblance to the analytical case gets better (closer resemblance between analytical result and precalculated result when increasing the amount of grids) when it comes to energy, kappa-value, pitch angle, and the appearance of the trajectory.

Scenario 3: Same as for Scenario 2. See Appendix 4 for the graphs of Scenario 3.

Scenario 4: The resemblance to the analytical case gets better for every increase in the amount of grids when it comes to magnetic moment. Concerning the energy and pitch angle, the result gets better with every increase except for the last one (27 times), when the tendency goes somewhat in the wrong direction.

Scenario 5: Same as for Scenario 2, except that the energy goes somewhat in the wrong direction for the case when the grid amount is 27 times the original amount.

Scenario 6: Because the particle goes out of the predefined boundary for all precalculated cases at an early stage, no conclusions regarding the development of the resemblance can be made.

Scenario 7: Because the particle goes out of the predefined boundary for all cases at an early stage, no conclusions regarding the development of the resemblance can be made.

Scenario 8: Same as for Scenario 5.

Scenario 9: Same as for Scenario 2, but the particle impacts for all precalculated cases.

Scenario 10: Same as for Scenario 7.

Scenario 11: Same as for Scenario 7, except that the particle impacts.

Scenario 12: Same as for Scenario 2.

Scenario 13: The resemblance decreases as the particle goes out of the predefined boundary as the amount of grids increases.

Scenario 14: No greater improvement in resemblance is detected.

Scenario 15: The results somewhat oscillate. The results of the normal grid amount show good a resemblance. It gets somewhat worse for the grid with 8 times the normal amount, and then gets better for the grid with 27 times the normal amount.

Scenario 16: The resemblance gets much better when increasing the amount of grids 27 times, as the particle goes out of the boundary for the other precalculated results. See Appendix 5 for the graphs of Scenario 16.

Scenario 17: Same as for Scenario 2, except that the magnetic moment gets somewhat worse when increasing the amount 27 times.

Scenario 18: Same as for Scenario 7.

3.4 Comparing the Polynomial Results with the Linear Results (Dynamic Magnetic and Electric Fields)

When comparing the polynomial results with the linear results, the results were almost identical. The only things that differed were the magnetic moment—where the linear result experiences an abrupt change, which is due to an abrupt change in the *E*-field—and/or possibly, the energy. For Scenario 8, the polynomial result showed an abrupt change in the kappa-value, which the linear result did not show. However, when increasing the time interval for the change between the two Tsyganenko levels to 600 s (instead of 60 s), the abrupt changes vanish. This is due to increasing the time interval that will make the curve much smoother and the transition less abrupt.

3.5 Dynamic Magnetic and Electric Fields

The comparison concerning a dynamic magnetic field showed a very good resemblance between the two cases. When trying to add a dynamic electric field, the mathematics at first posed a problem. The comparison did not show enough resemblance between the two cases. The problem was finally solved and when comparing the results of a dynamic magnetic and electric field, the results of the precalculated case showed a very good resemblance with the analytical results. Satisfactory results were, therefore, achieved regarding a dynamic magnetic and electric field.

4. Conclusions

The results from the particle motion in an interpolated magnetic field and particle motion in interpolated magnetic and electric fields showed a very good resemblance; therefore, we can be confident when it comes to executing MHD-simulations (with respect to interpolating simulations). A 0lot of time can be saved by using interpolation—instead of time consuming analytical simulations—in these cases.

The sensitivity analysis—for the particle motion in interpolated magnetic field and particle motions in interpolated magnetic and electric fields—in general show large improvements in accuracy between the analytical results and the precalculated results with an increased number of grid points. In some cases, more or less identical results between the analytical and the precalculated simulations were found. The decreased accuracy concerning energy could be explained with the random nature of the particle trajectories. Weighing the simulation time (the simulations take longer when increasing the number of grids) and the resulting accuracy, an optimal number of grids would probably be eight times the original number.

The few things that differed when comparing the polynomial results with the linear results—dynamic magnetic and electric fields—were generally easily corrected by increasing the time interval between the change of the Tsyganenko levels. By doing so, the time interval will make the curve much smoother and the transition less abrupt.

The comparison concerning a dynamic magnetic field showed a very good resemblance between the two cases, but when trying to add a dynamic electric field, the mathematics posed a problem. The comparison did not show enough resemblance between the two cases. The problem was how to calculate the expression given by

$$\int (E_i \bullet B) ds \,, \tag{16}$$

without field line tracing. Equation (16) is found in the expression for the total *E*-field, given by

$$E = -\nabla (P + \int (E_i \bullet B) ds) + E_{i\perp} \,, \tag{17}$$

where P is the electrostatic potential (obtained from mapping to the ionosphere), E_i is the inductive electric field and B is the magnetic field.

The problem was solved in the following way: the total *E*-field was precalculated during the transition between the two levels, calculating the *E*-field at a 3 second interval. The particle trajectory was calculated by doing temporal and spatial interpolation to find the *E*-field at a particular time and location along the trajectory. When comparing the results of a dynamic magnetic and electric field, a very good resemblance with the analytical results was found; thus, satisfactory results were achieved regarding a dynamic magnetic and electric field.

References

[1] Kivelson, M.G., et al., (1997). *Introduction to Space Physics.* New York: Cambridge University Press.

[2] Lundin, R., (1998). *Föreläsningsanteckningar Rymdfysik.* Kiruna: Institutet för Rymdfysik.

[3] Moore, T.E., et al., (2004). *Plasma Sheet and (Non-Storm) Ring Current Formation from Solar and Polar Wind Sources.* tem692.gsfc.nasa.gov/public/Moore-PSformation-rev1/0-Moore-PSRCform-R2V0.pdf 10/25/2005.

[4] Chapman, S.J., (2004). *Fortran 90/95 for Scientists and Engineers.* Singapore: McGraw-Hill.

[5] Gumley, L.E., (2002). *Practical IDL Programming.* San Diego: Academic Press.

[6] Delcourt, D.C., et al., (1988). *Low-energy Bouncing Ions in the Magnetosphere: a Three-Dimensional Numerical Study of Dynamic Explorer 1 Data. Journal of Geophysical Research*, volume 93, 1988.

[7] www.uaf.edu/asgp/hex/ionosphere.htm 07/17/2005.

[8] en.wikipedia.org/wiki/Magnetic_reconnection 07/17/2005.

[9] science.nasa.gov/HSVWorkshop/sessions.asp 07/17/2005.

[10] Volland, H., (1978). *A Model of the Magnetospheric Convection Electric Field. Journal of Geophysical Research*, volume 83, pp 2695–2705.

[11] Delcourt, D.C., et al., (1990). *Dynamics of Single-Particle Orbits During Substorm Expansion Phase. Journal of Geophysical Research*, volume 95, pp 20,853–20,865.

[12] Tsyganenko, N.A., (1989). *A Magnetospheric Magnetic Field Model with a Warped Tail Current Sheet. Space Science Review*, volume 37, No. 1, pp 5–20.

[13] Delcourt, D. C. et al.,(1996). *Centrifugally Driven Phase Bunching and Related Current Sheet Structure in the Near-Earth Magnetotail*. *Journal of Geophysical Research*, volume 101, pp 19,839–19,847.

Appendix 1

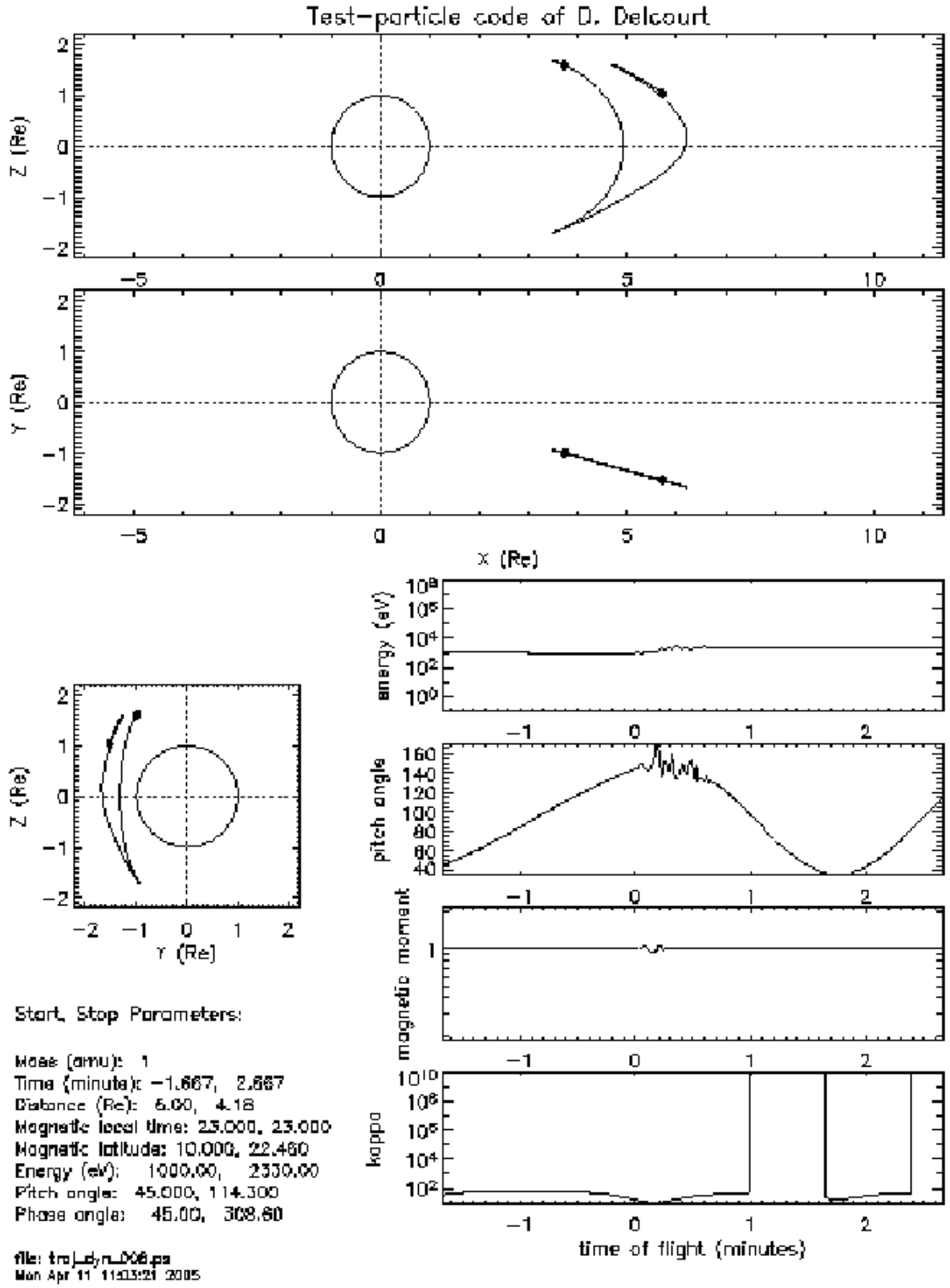

Figure A1. Polynomial transition, Scenario 8.

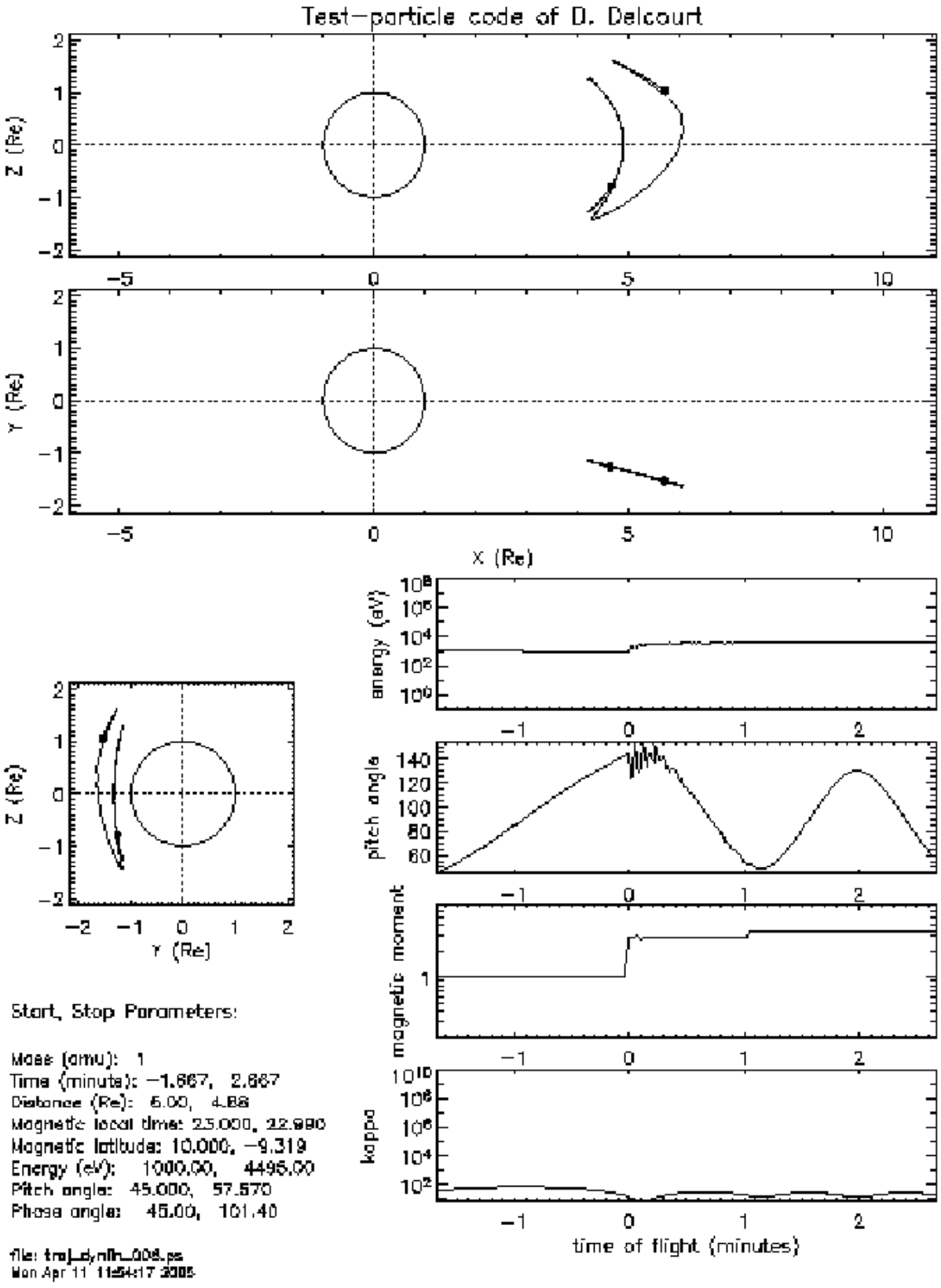

Figure A2. Linear transition, Scenario 8.

Appendix 2

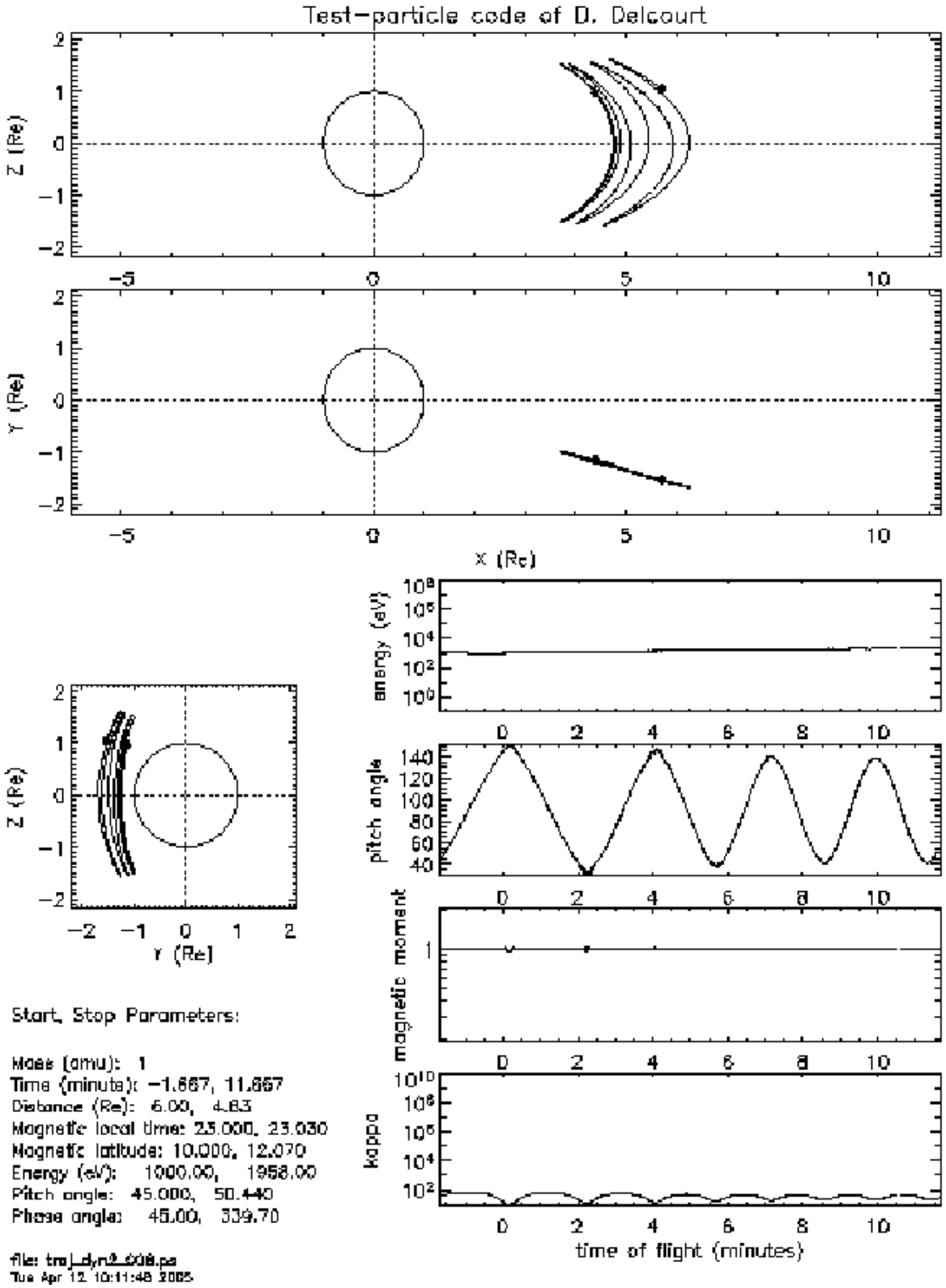

Figure A3. Polynomial transition, Scenario 8. Increasing the time interval to 600.

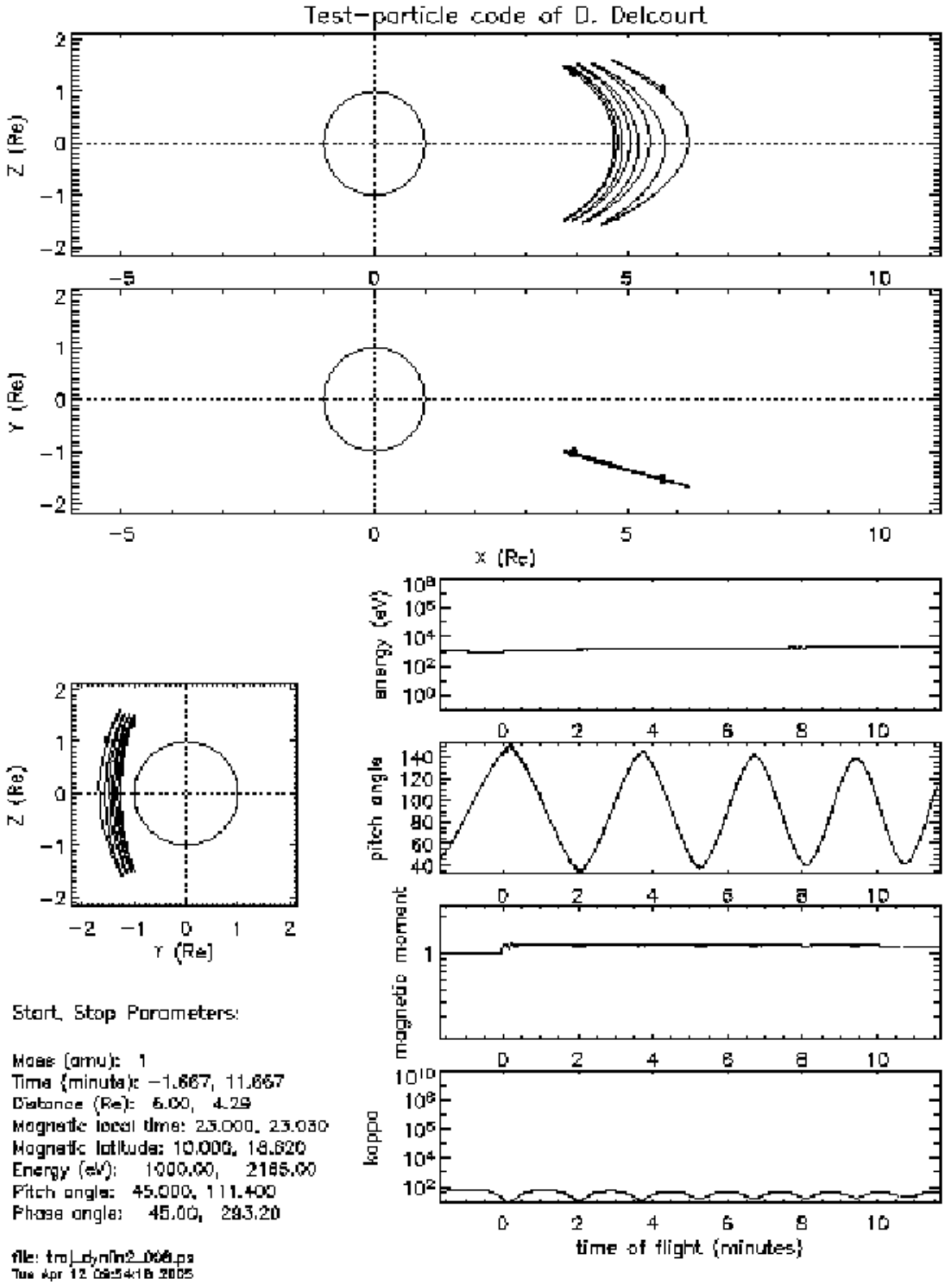

Figure A4. Linear transition, Scenario 8. Increasing the time interval to 600.

Appendix 3.

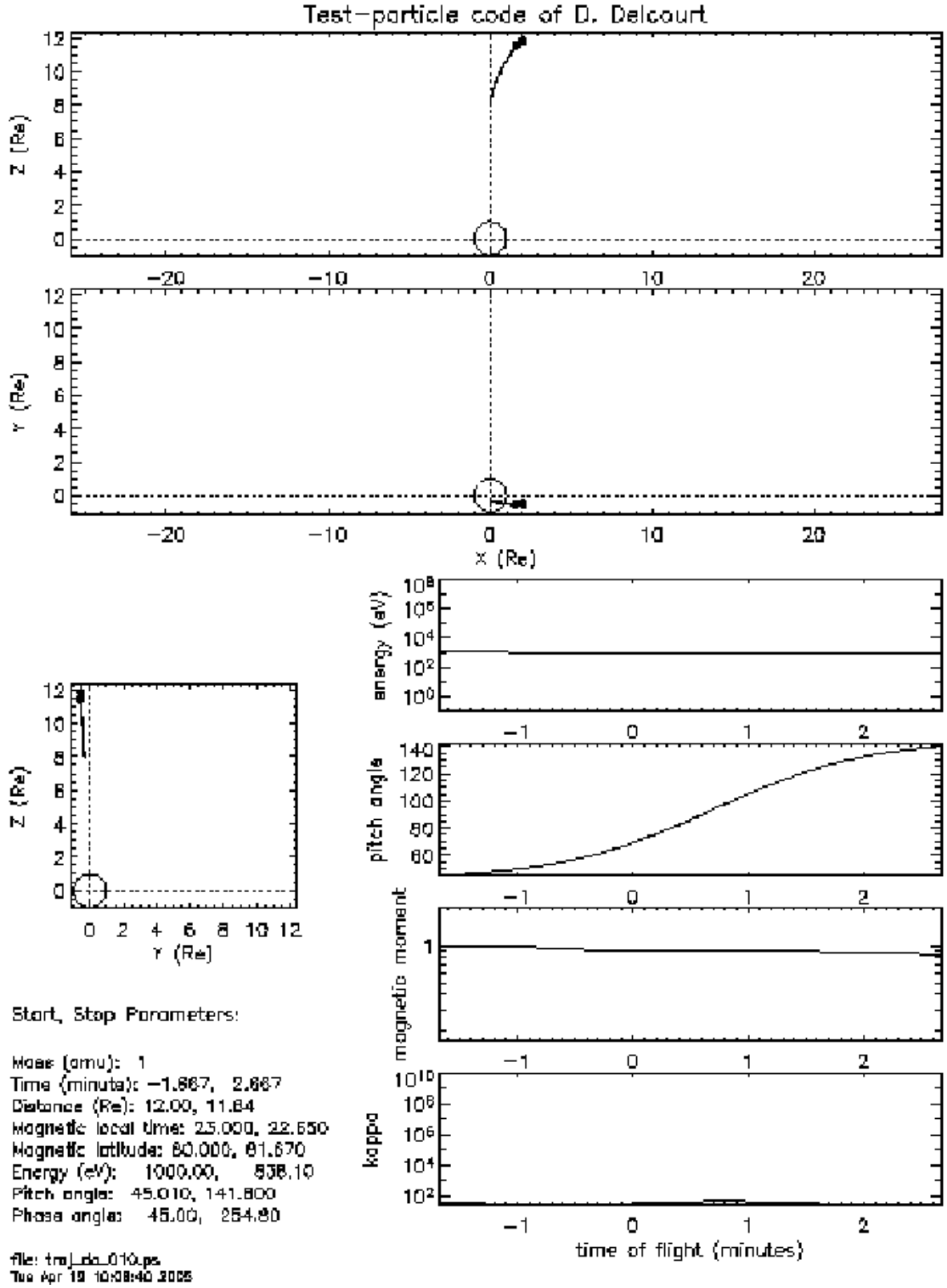

Figure A5. Analytical case for Scenario 10.

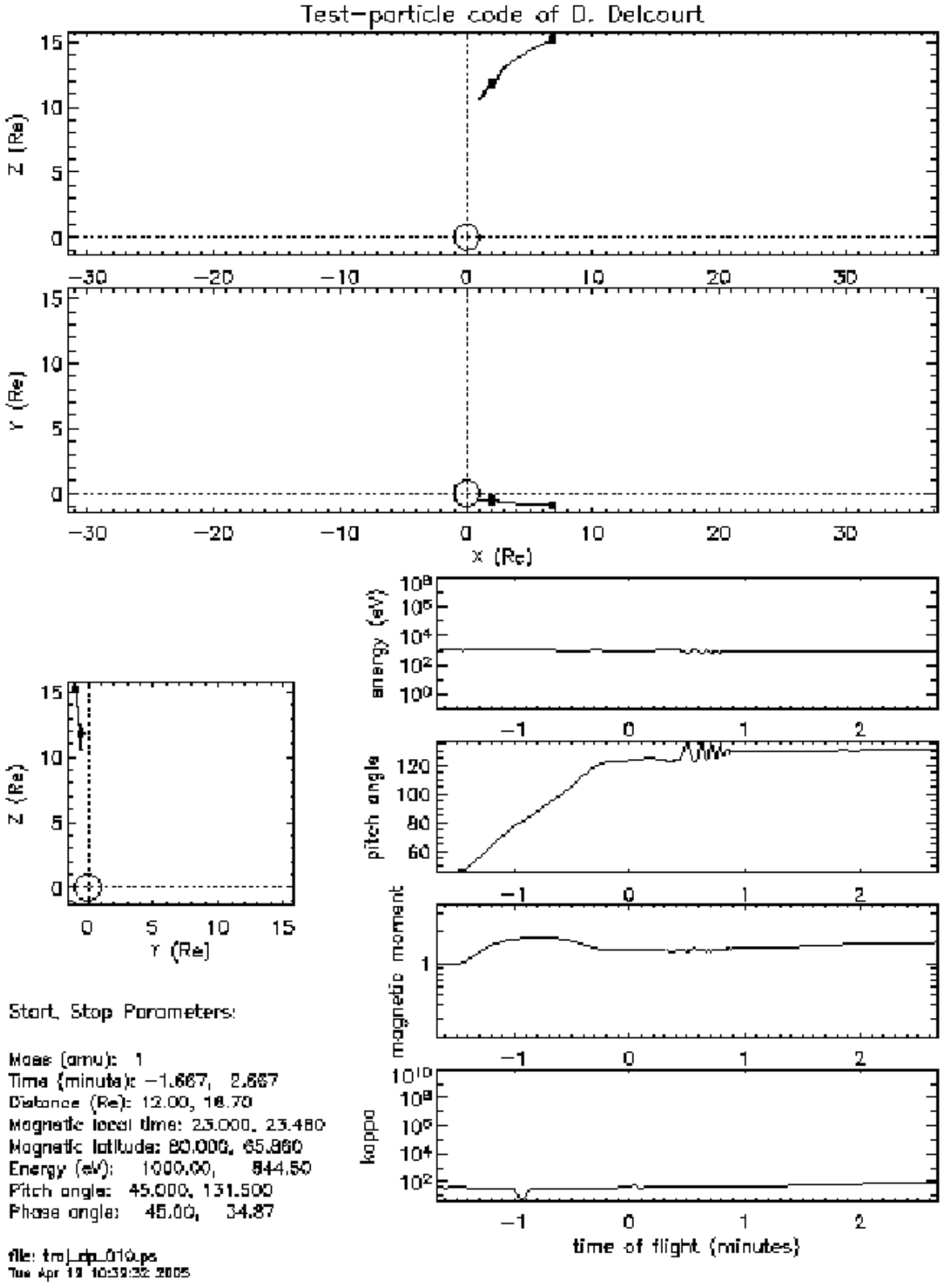

Figure A6. Precalculated case for Scenario 10.

Appendix 4.

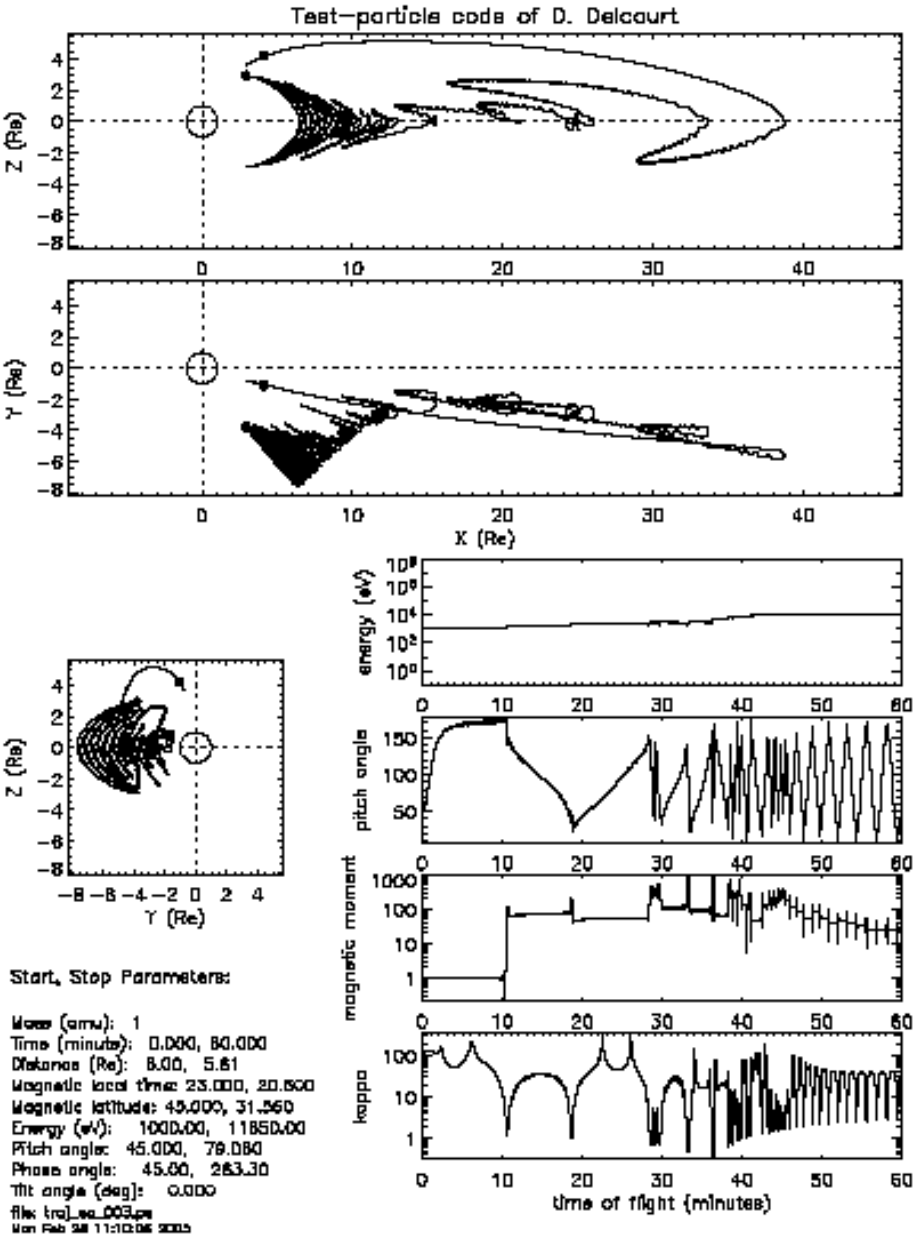

Figure A7. Analytical case (Scenario 3).

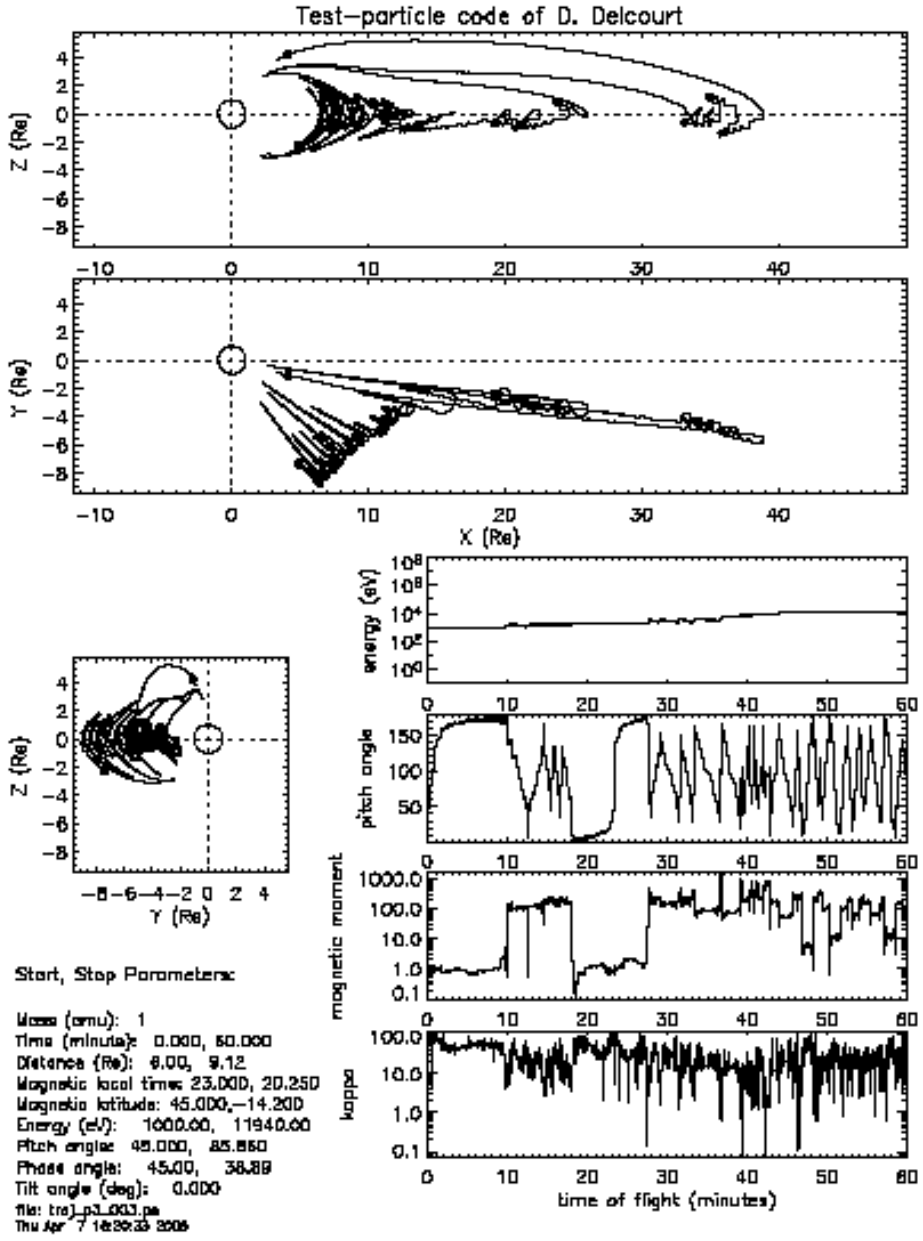

Figure A8. Precalculated case with original grid numbers (Scenario 3).

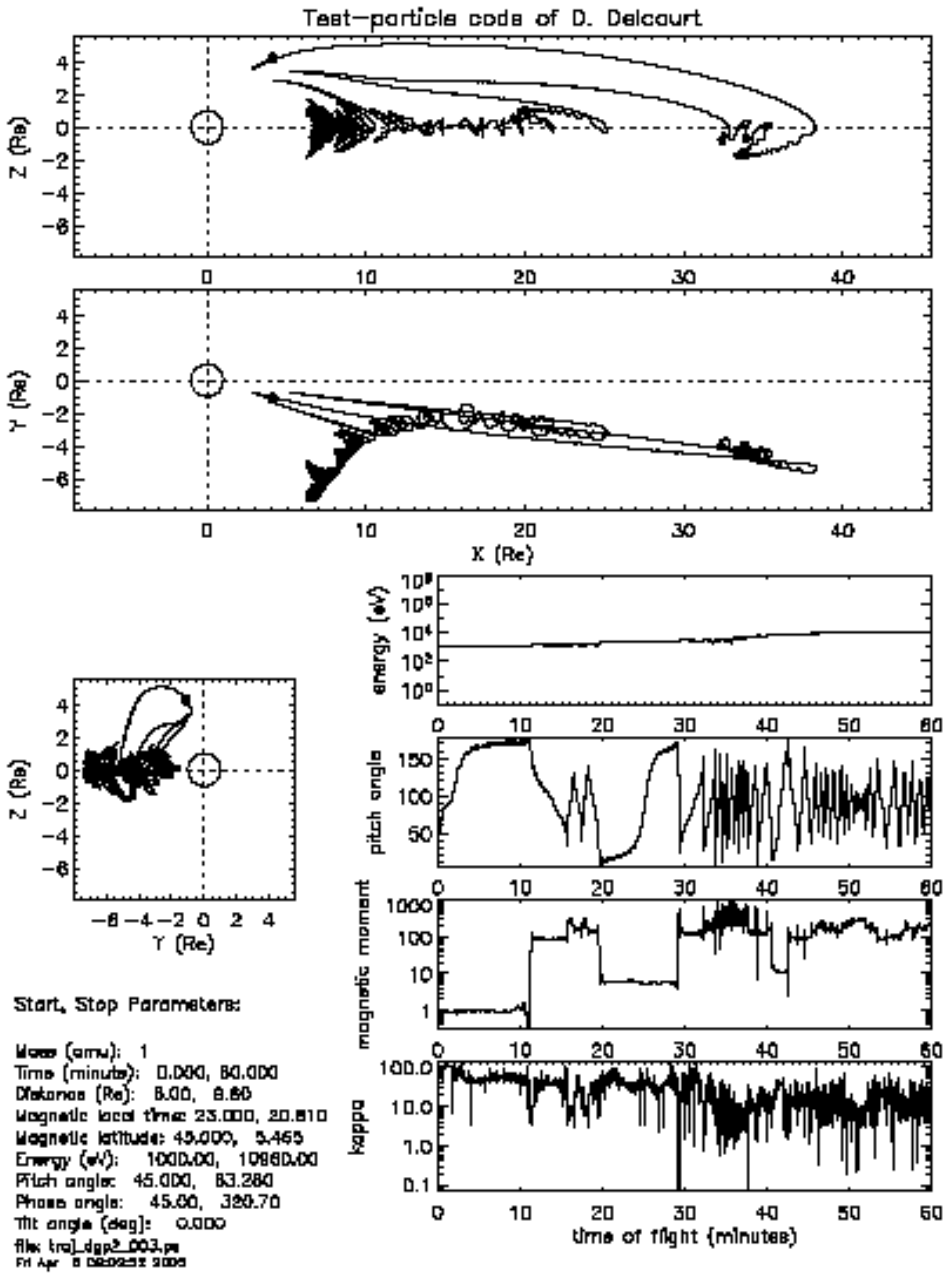

Figure A9. Precalculated case with 8 times the number of grids (Scenario 3).

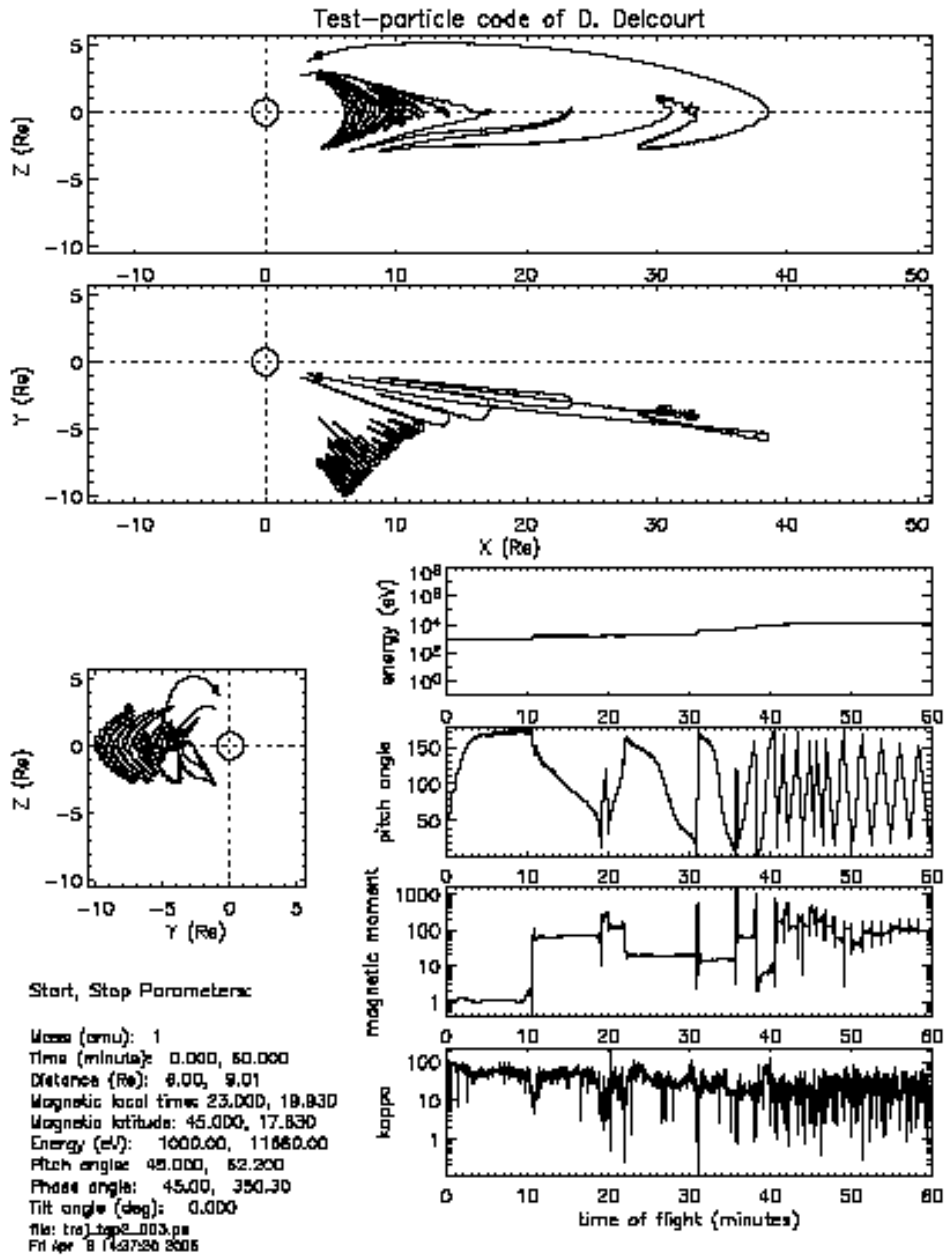

Figure A10. The precalculated case with 27 times the number of grids (Scenario 3).

Appendix 5.

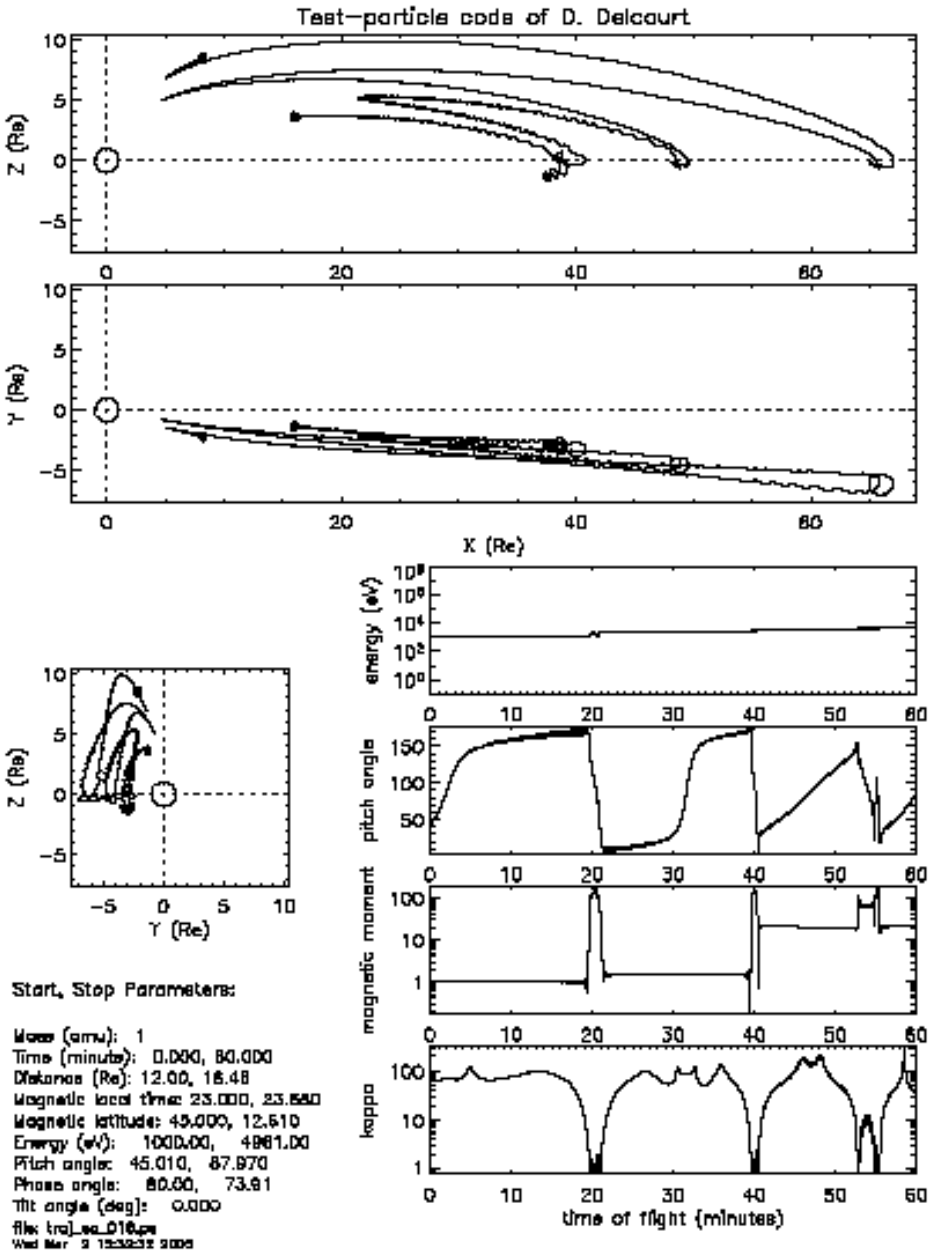

Figure A11. Analytical case (Scenario 16).

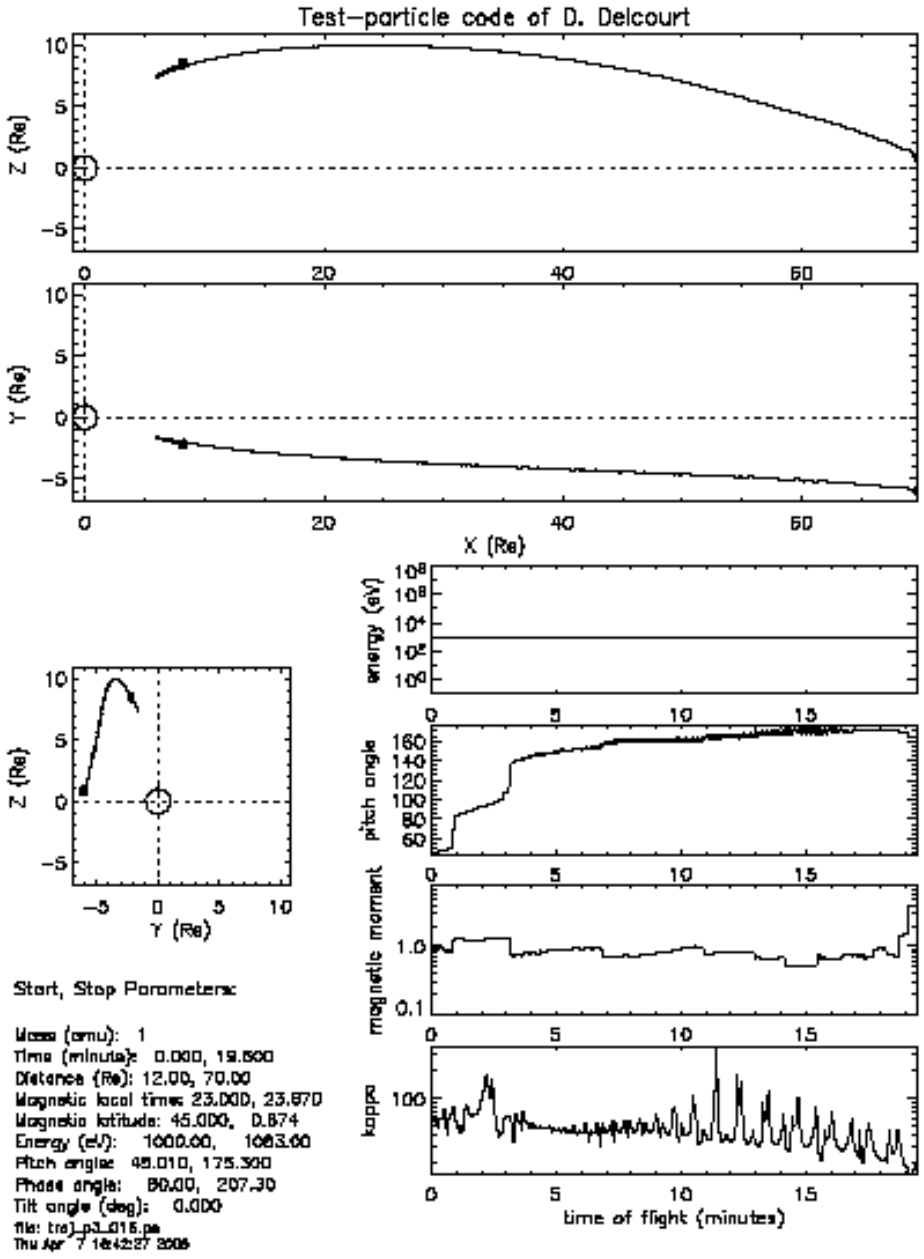

Figure A12. Precalculated case with original grid numbers (Scenario 16).

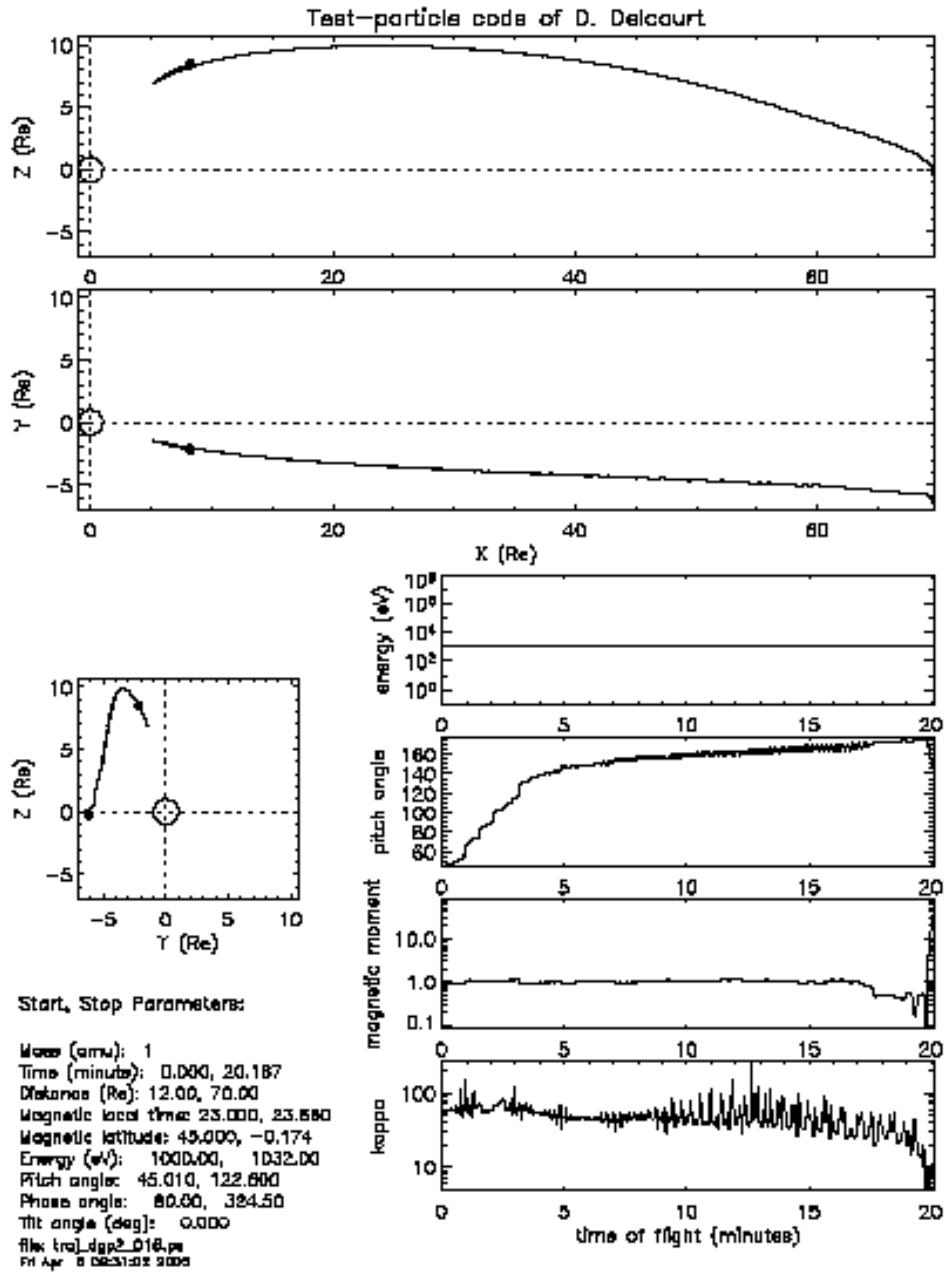

Figure A13. Precalculated case with 8 times the number of grids (Scenario 16).

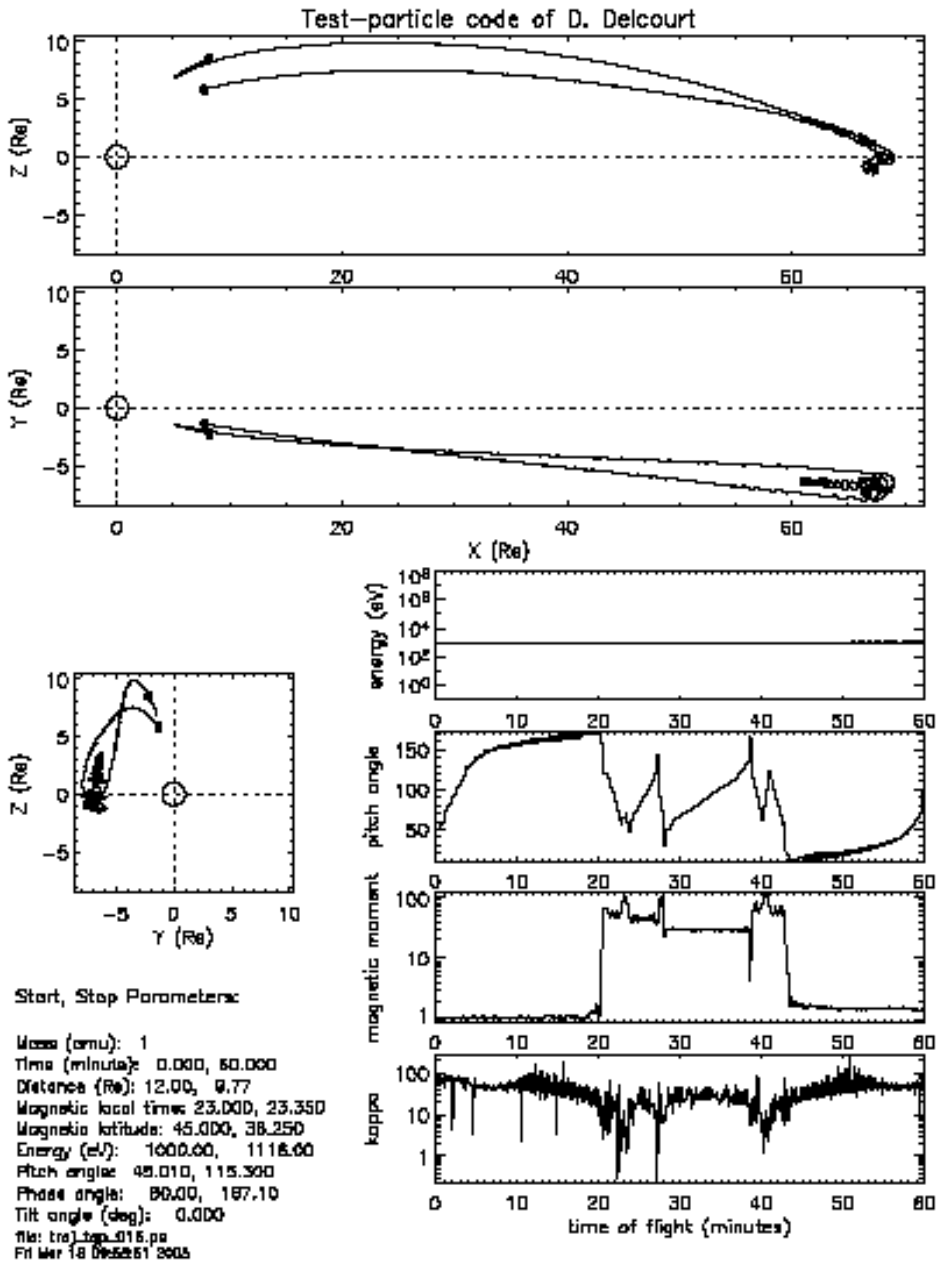

Figure A14. Precalculated case with 27 times the number of grids (Scenario 16).

REPORT DOCUMENTATION PAGE

Form Approved
OMB No. 0704-0188

1. REPORT DATE *(DD-MM-YYYY)*	2. REPORT TYPE	3. DATES COVERED *(From - To)*
27-12-2006	Technical Memorandum	

4. TITLE AND SUBTITLE

Effects of Finite Element Resolution in the Simulation of Magnetospheric Particle Motion

5a. CONTRACT NUMBER

5b. GRANT NUMBER

5c. PROGRAM ELEMENT NUMBER

6. AUTHOR(S)

Rickard Hansen

5d. PROJECT NUMBER

5e. TASK NUMBER

5f. WORK UNIT NUMBER

7. PERFORMING ORGANIZATION NAME(S) AND ADDRESS(ES)

Goddard Space Flight Center
Greenbelt, MD 20771

8. PERFORMING ORGANIZATION REPORT NUMBER

2006-02036-0

9. SPONSORING/MONITORING AGENCY NAME(S) AND ADDRESS(ES)

National Aeronautics and Space Administration
Washington, DC 20546-0001

10. SPONSORING/MONITOR'S ACRONYM(S)

11. SPONSORING/MONITORING REPORT NUMBER

TM-2006-214148

12. DISTRIBUTION/AVAILABILITY STATEMENT

Unclassified-Unlimited, Subject Category: 46
Report available from the NASA Center for Aerospace Information, 7115 Standard Drive, Hanover, MD 21076. (301) 621-0390

13. SUPPLEMENTARY NOTES

14. ABSTRACT

This document describes research done in conjunction with a degree program. The purpose of the research was to compare particle trajectories in a specified set of global electric and magnetic fields; to study the effect of mesh spacing, resulting in an evaluation of adequate spacing resolution; and to study time-dependent fields in the context of substorm dipolarizations of the magnetospheric tail.

15. SUBJECT TERMS

Ionosphere, Magnetosphere, Magnetic Reconnection, Magnetotail, Interpolation, Dynamic Field, Electric Field, FORTRAN, Delcourt

16. SECURITY CLASSIFICATION OF:			17. LIMITATION OF ABSTRACT	18. NUMBER OF PAGES	19b. NAME OF RESPONSIBLE PERSON
a. REPORT	b. ABSTRACT	c. THIS PAGE			Thomas Moore
Unclassified	Unclassified	Unclassified	Unclassified	49	19b. TELEPHONE NUMBER *(Include area code)* (301) 286-5236